MAY 2001 ECN-C--00-077

NM3000 - LMH46-5 BLADE DESIGN

Aerodynamic Parameter Sensitivity Study

C. Lindenburg E. Bot H.B. Hendriks

Acknowledgement

The work reported here is carried out within the DOWEC research and development project. This project is funded partly by the EET program under number EETK98031/398410-0810.

This work was possible thanks to the contribution of Eric van der Hooft in providing control algorithms for several configurations.

For the configuration with low turbulence, representing sea climate, the authors wish to express their appreciation to Terry Hegberg.

Abstract

An investigation is carried out into the LMH46-5 rotor blade geometry that combines a high annual energy capture with relatively low values for the extreme blade root and tower base moments. Within this investigation the load spectrum is calculated for several configurations that have variations in airfoil characteristics, blade chord, blade taper ratio and rotor speed. Furthermore some configurations with differences in structural properties and with a low turbulence intensity are analysed. For most of the configurations the blade twist is optimised with the program BOT to obtain a maximum energy capture for a Weibull wind distribution with an average of 9m/s. For each configuration the annual energy capture was integrated from the quasi-stationary power curve calculated with PHATAS-IV, also with a Weibull average of 9m/s and an IEC turbulence intensity of 12%.

For most of the configurations the dynamic load set was calculated for each of the aerodynamic variations in blade design with a turbulence intensity of 16%. From these dynamic load sets, the extreme and fatigue moments in the blade root, rotor shaft and in the tower base were selected, while also the 'dynamic energy capture' was integrated from the dynamic load sets.

The results are presented as relative variations with respect to the so-called "baseline" configuration, named *C-00*. The baseline configuration has the "LMH46-5-X00" rotor blades. Finally the cost of energy is calculated for the configurations using component-cost estimates as function of fatigue and extreme loads.

Keywords

Aerodynamic optimisation Cost of energy Dynamic loads PHATAS program Price Performance ratio Sensitivity analysis Wind turbine

CONTENTS

1.	INTRODUCTION 1.1 General
2.	PARAMETRIC VARIATIONS 2.1 Configurations with Baseline Geometry 2.2 Variations of the Rotor Solidity 2.3 Variations of Rotational Speed 2.4 Variations of Taper Ratio 2.5 Configurations with the LMH46-5-X60 Blade Geometry 2.6 Differences in Structural Aspects 1 Influence of Off-shore Locations 1
3.	WIND TURBINE SETTINGS 3.1 Controller Settings
4.	COMPARISON 1 4.1 Calculated Power Production 1 4.2 Extreme Loads 1 4.2.1 Extreme rotor speed 1 4.2.2 Extreme tower base moments 1 4.2.3 Extreme tower top moments 2 4.2.4 Extreme shaft moments 2 4.2.5 Extreme blade root moments 2 4.2.6 Extreme flatwise blade moments 2 4.2.7 Minimum tower clearance 2 4.3 Fatigue Loads 2 4.3.1 Tower fore-aft loads 2 4.3.2 Tower side loads 2 4.3.3 Non-rotating shaft loads 2 4.3.4 Rotating shaft moments 3 4.3.5 Blade loads 3
5.	ESTIMATED COST OF ENERGY 5.1 Cost Estimation as Function of Design Loads 5.2 Cost of Energy for each Configuration 5.3 Cost of Energy versus Blade Chord 5.4 Cost of Energy versus Rotor Speed 5.5 Cost of Energy versus Effective Solidity 3 3 3 3 3 3 3 3 3 3 3 3 3
6.	INFLUENCE OF STRUCTURAL BLADE PROPERTIES 6.1 Influence of Bending Stiffness
7.	CONCLUSIONS 4

NM3000 - LMH46-5 BLADE DESIGN

7.2	Load set Calculations	43
7.3	Aerodynamic Optimisation	44
7.4	Aerodynamic Parameter Variations	45
7.5	Cost of Energy	46
7.6	Structural Parameter Variations	46
REFER	ENCES	47
APPEN	DIX A. OPTIMUM BLADE GEOMETRY	49
A.1	Blade Chord	49
A.2	Blade Twist	49
A.3	Optimised Parametric Geometry	50
APPEN	DIX B. CALCULATION METHODS FOR ANNUAL YIELD	51
APPENI	DIX C. ROTOR BLADE SCALING RELATIONS	55

1. INTRODUCTION

1.1 General

Within the Dutch DOWEC project an investigation is performed into turbines for offshore applications. This project is addressed both to the development of large wind turbines for offshore locations and to the investigation into different turbine concepts. One of the turbines to be developed is the 3MW NM3000 wind turbine, which is described in [7]. This turbine has a 96m diameter 3-bladed rotor and a variable speed generator concept for which the rotor speed above nominal wind is controlled by active blade pitching. For the design of this turbine several configurations with variations in blade design are analysed by load-set calculations with the program PHATAS-IV. In the remainder of this report the name PHATAS refers to PHATAS-IV release "DEC-1999", [11].

This document describes the aerodynamic variations of the LMH46-5-X00 rotor blade, specified in [2], for the NM3000 wind turbine including a comparison of annual energy capture and design and fatigue loads. In chapter 2 these configurations are described in terms of the differences with respect to the baseline configuration 'C-00' of which the blade model is described in [13].

For configurations having different aerodynamic rotor characteristics specific parameters for the control algorithm are determined. Since most parameter variations have consequences on the aerodynamic operational state of the rotor, the generator characteristics and the blade pitch angle for partial load operation are adjusted. A description of these adjustments and the corresponding quasi-stationary prediction of the annual yield is given in chapter 3.

After having calculated the IEC design load cases [9], the annual energy capture is integrated from these load time series while the extreme and fatigue equivalent loads are retrieved for a number of cross sections in the rotor blades, shaft and tower. The results are presented in chapter 4.

With parametric cost estimates as function of the structural loads the price-performance ratios are calculated and reported in chapter 5.

Especially variations in blade chord will imply structural modifications giving variations in blade bending stiffness. The influence of blade bending stiffness for a given aerodynamic configuration is investigated by performing dynamic load calculations for normal operation at 12m/s. The extreme and fatigue equivalent loads for this investigation are presented in chapter 6.

The design of a rotor blade always balances between large airfoil thickness, giving an efficient structure, and a small thickness giving a smaller aerodynamic drag. An investigation to the influence of variations in mass and stiffness distribution due to thickness variations is performed and also included in chapter 6.

After performing this study, considerations on the optimisation of the blade chord and twist distribution are written in appendix A.

Because the cost of energy depends strongly on the calculated annual energy production, an investigation is done to the energy yield as function of the 'effective solidity' (see page 17) calculated with different methods. The differences show the influence of analysis method, and are reported in appendix B.

To some extent the influence of a number of design parameters can be derived analytically. For design parameters such as 'diameter', 'rotor speed' or 'tip speed ratio' and 'blade chord' the influence on the structural loads and the dynamic properties of the turbine is expressed and listed in appendix C.

1.2 Conditions

The external conditions and internal turbine parameters that are used for the calculation of the energy capture differ from those for the dynamic loads. In addition to the "stationary-" versus "stochastic-" or "transient-" wind conditions, these differences are:

- Turbulence intensity; Vertical shear profile; Pitch error;
- Radius of tip vortex; Yaw misalignment.

1.3 Optimised Baseline

The baseline configuration for which a CD-rom with the load set was distributed (July 2000) has a blade twist distribution that was optimised for a 95m rotor diameter and a 15.08rpm rotor speed. After the increase in rotor diameter and corresponding decrease in rotor speed (for a given tip speed of 75m/s) and also after gaining more experience on finding the optimised blade twist, the twist distribution of all other blade configurations have different characteristic shapes. For a fair comparison, the twist of the LMH46-5-X00 blade, see [2] was again optimised and used in this report as baseline configuration *C-00*. The configuration *C-01* of which a CD-rom was distributed on July 3, 2000 and of which a full description is given in the confidential "baseline" report ECN-CX--00-077 [13] is treated here as one of the variations. The latter report contains absolute data of configuration *C-01*.

1.4 Modification of Load Cases Compared to the Baseline

After distributing the CD-rom (on July 3, 2000) with the load set for the LMH46-5-X00 "baseline" blade, some reactions were received that led to modifications of some load cases:

DLC 5.1 Emergency shut down;

For each configuration the over-speed level for triggering the brake is adjusted such that the 10deg/s brake action takes place.

DLC 6.2 Stand by above cut-out wind speed;

For configuration *C-01* the dynamic loads above cut-out wind speed were calculated (in June 2000) for turbulent wind with an average of 35m/s and were written in file 620. It appeared that these loads have a significant contribution to the fatigue-equivalent load cycles, which can be reduced if the wind velocity above the cut-out wind is described with four intervals with an average wind speed of 30m/s, 35m/s, 40m/s and 45m/s. The loads for these conditions are stored in files 630, 635, 640 and 645. The time in which these loads add to the fatigue equivalent load cycles is according to the Weibull probability that the wind is between 25-30, 30-35, 35-40, and above 40m/s for the files 630, 635, 640 and 645 respectively. For the estimated cost of energy, chapter 5, the extreme loads are calculated without this load case, assuming that the free-yawing mechanism is designed to reduce the dynamic response.

DLC 7.1 Parked at 1-year extreme wind with blades in working position;

For the 'former baseline' (June 2000) these loads were calculated with a fixed rotor speed of 4rpm in order to cover many rotor positions. For this rotor speed the calculated extreme loads were rather large.

It was thus decided to repeat these calculations with a smaller rotational speed of 2rpm.

These modifications are issued for all load cases within the aerodynamic sensitivity study. For fair comparison they are also issued for the former baseline configuration *C-01*.

Based on preliminary results of this investigation, LM Glasfiber decided to continue their development for the configuration named C-21. For this reason the airfoil coefficients for this configuration are adjusted for the real Reynolds number of the rotor blades which is about $7 \cdot 10^6$.

2. PARAMETRIC VARIATIONS

For the NM3000 turbine with LMH46-5-X00 rotor blades the annual power production and the dynamic loads are calculated for a number of variations of the configuration. Most of these configurations have variations in aerodynamic properties. Because some configurations have the same blade design, it was found necessary to use a unique configuration number in the underlying report.

The configuration of the "baseline" with LMH46-5-X00 rotor blades is called *C-00*. A description of the LMH46-5-X00 rotor blades with the non-optimised twist (config. *C-01*) is given in [2].

For most configurations the blade twist distribution is optimised for maximum energy capture, with the **B**lade **O**ptimisation **T**ool BOT [1] for a Weibull wind distribution with an average of 9m/s (Weibull scale 10.155m/s) and a Weibull shape parameter of 2.

The optimised twist is also calculated for the configurations with LMH46-5-X00 rotor blades. The configurations that do not have an optimised twist are marked with '*n.o.t.*'.

The configurations can be grouped on basis of parametric variations, among which relative blade chord (solidity), tip speed ratio, taper ratio and others (e.g. structural variations). Each group of configurations is described in one of the following sections.

2.1 Configurations with Baseline Geometry

C-01: LMH46-5-X00, Former baseline

Initially the rotor-speed for the NM3000 was 15.08rpm, based on a maximum tip speed of 75m/s and a rotor diameter of 95m. The diameter of the LMH46-5 rotor blade finally was somewhat larger which was the reason to reduce the rotor speed to 14.92rpm. For this configuration the dynamic load set was calculated and distributed on CD-rom on July 3, 2000.

Investigations with the program BOT showed that optimising the twist for this decreased rotor speed results in a higher energy capture. The blade with this optimised twist (C-00) is used here as 'baseline' while the twist of configuration C-01 (analysed and distributed on July 3, 2000) is not optimised. As a result of the reduction in rotor speed the 'baseline' blade chord is $80\%*(95/96)^2 = 78.34\%$ of the 'aerodynamic optimum'.

C-02: LMH46-5-X03: DU 96-W-180 airfoils at the tip

The outer part of the baseline blade has NACA64-618 airfoils. For configuration C-02 (LMH46-5-X03 blade) these airfoils are replaced by the (also 18% thick) DU 96-W-180 airfoils. Ruud van Rooij prepared the coefficients for these airfoils for a Reynolds number of $3 \cdot 10^6$, see figure 2.1. Because the angle of attack for optimum c_1/c_d is airfoil-dependent also here the twist is optimised.

C-03: LMH46-5-X00, NACA63-618 airfoils at the tip

For configuration C-03 the NACA64-618 airfoils are replaced by the NACA63-618 airfoils. The coefficients for these airfoils are prepared by Ruud van Rooij for a Reynolds number of $3 \cdot 10^6$, see figure 2.1.

2.2 Variations of the Rotor Solidity

Compared to the blade geometry for a maximum annual yield, a blade geometry with a somewhat smaller chord gives a direct reduction of the structural loads and a minor (second order) reduction in annual yield. For this reason the blade chord of the 'baseline' is already reduced to 78.34% of the chord for maximum energy yield. The following configurations are addressed to the influence of blade-chord or 'solidity' on the energy capture and on the structural loads.

C-04: 80% slender chord

The blade chord of the baseline blade LMH46-5-X00 is decreased with 20% giving this 'slender' geometry. This blade chord is 62.67% of the chord for maximum yield. This configuration is analysed with airfoil coefficients that are prepared for the aspect ratio of the 90% slender configuration *C-05*.

For this configuration no load spectrum is calculated.

C-05: LMH46-5-X01: 90% slender chord

The blade chord of this 'slender' configuration is reduced to 90% of the LMH46-5-X00 chord, see [3]. This chord is 70.51% of the chord for maximum yield.

With this reduced chord also the aspect ratio of the blade is increased. In the PHATAS model the aspect ratio is calculated for the part of the blade outside of the root vortex radius. Since the diameter of the root flange is *not* reduced, the radius of the root vortex appears to be smaller giving an aspect ratio of 18.15. For a fair comparison with the baseline blade (aspect ratio 15.5) the airfoil coefficients in deep stall are calculated for an aspect ratio of 15.5/0.9 = 17.222.

The files with airfoil coefficients for this aspect ratio include the character string 'X01'.

C-06: LMH46-5-X01: 90% slender chord, 81% stiffness

For a smaller chord with the same relative airfoil thickness the cross section has less bending stiffness when the same amount of material is used. Assuming that the extreme wind pressure on the blade surface gives dimensioning loads, appendix C shows that the same amount of cross sectional material is needed and that the bending stiffness is proportional to the chord squared. Because the mass and thus the rotor inertia remains the same, this does not have consequences for the control algorithm. Another load set was prepared with the stiffness reduced to 81%.

C-07: LMH46-5-X02: 110% wide chord

The blade chord of this 'wide' configuration is increased to 110% of the LMH46-5-X00 chord, which is 86.18% of the chord for maximum yield. A description of the LMH46-5-X02 blade is given in [4]. As for the 'slender' configuration C-05 the aerodynamic coefficients in deep stall are calculated for an aspect ratio of 15.5/1.1 = 14.091.

The files with airfoil coefficients for this aspect ratio include the character string 'X02'.

C-08: LMH46-5-X02: 110% wide chord, 121% stiffness

In contrast with the slender blade, the wider X02 blade will finally lead to an increased stiffness because of the wider chord. The load set for this configuration is analysed also, using the same controller parameters as for configuration *C-07*.

C-09: 120% wide chord

The blade geometry of the baseline blade LMH46-5-X00 is increased with 20% giving this wide geometry. This chord is 94.01% of the chord for maximum yield. As for the configuration *C-04* with the 80% slender blade the twist for this 120% blade is optimised with BOT from which only the annual energy capture is included in this report.

2.3 Variations of Rotational Speed

C-10: LMH46-5-X00, 86.6% sub-optimal speed, non-optimised twist

Over the entire operational range the rotor speed is 86.6% of the speed for the baseline C-00, aiming at about 4% loss of production. Configuration C-10 is analysed with the twist of the baseline 'X00' blade.

C-11: LMH46-5-X00, 86.6% sub-optimal speed, optimised twist

Similar as configuration *C-10* but with an optimised twist.

C-12: LMH46-5-X00, 90.3% sub-optimal speed, non-optimised twist

Over the entire operational range the rotor speed is 90.3% of the speed for the baseline C-00 (about 2% production loss). Configuration C-12 is analysed with the twist of the baseline 'X00' blade.

C-13: LMH46-5-X00, 90.3% sub-optimal speed, optimised twist

Similar as configuration *C-12* but with an optimised twist.

C-14: LMH46-5-X00, 93.3% sub-optimal speed, non-optimised twist

Over the entire operational range the rotor speed is 93.3% of the speed for the baseline *C-00* (about 1% production loss). Configuration *C-14* has the twist of the baseline 'X00' blade. For this configuration the dynamic load set is not calculated.

C-15: LMH46-5-X00, 93.3% sub-optimal speed, optimised twist

Similar as configuration *C-14* but with an optimised twist.

For this configuration also the dynamic load set is calculated.

C-16: LMH46-5-X00, Maximum tip speed 80m/s

For this configuration the maximum tip speed is increased from 75m/s to 80m/s compared to the baseline *C-00*. Here the improvement in annual energy capture is small.

For this configuration no dynamic load set is calculated.

C-17: Maximum tip speed 79m/s, 95% slender chord

For an increased rotor speed with the same blade geometry (as for configuration C-16) the chord distribution is closer to the value for the maximum yield, see appendix C. From the fact that the chord distribution is close to this optimum it can be foreseen that the annual energy capture for a higher speed is slightly larger than the baseline while the dynamic load variations will increase roughly linear with rotor speed. For this reason the blade chord can be reduced for a higher tip speed without much loss of power and with a reduction of extreme loads. The tip speed ratio for maximum energy capture appears to be near 7.9 which corresponds to a maximum tip speed of 79m/s. To compensate partially for the higher rotor speed the chord for configuration C-17 is reduced with 5% compared to the baseline. The resulting chord finally is 82.6% of the value for maximum yield.

C-18: Maximum tip speed 79m/s, 90% slender chord

Similar as for configuration *C-17* the tip speed is increased to 79m/s while the blade chord is reduced. Following appendix C the product of rotational speed squared and blade chord must be constant for the same rotor disk loading. For configuration *C-18* the blade chord distribution is 90% compared to the baseline, which is equal to the chord distribution of configuration *C-05*.

2.4 Variations of Taper Ratio

The 'slender' and 'wide' configurations with X01 and X02 blades are addressed to the effect of the total blade surface on the energy capture and the dynamic loads. However, the tip chord and the root chord may have a different influence on the design loads. A smaller tip chord is expected to give smaller flatwise bending moments over the blade span, while the maximum asymmetric loads will be reduced giving smaller shaft bending moments.

C-19: Tapered modification 1 of LMH46-5-X00

For configuration *C-19* the chord distribution is obtained by multiplying the LMH46-5-X00 chord distribution with a linear function that gives a 10% increase at the rotor centre (if extrapolated) and a 5% decrease at the blade tip. Compared to the 'maximum-yield geometry' this is a decrease of 13.8% at the rotor centre and 25.6% at the tip. Up to the largest chord, the chord distribution is the same as for the LMH46-5-X00 blade. Finally the total blade surface is 0.30% larger as for the baseline *C-00* while the radius-weighted blade surface is 0.27% smaller.

C-20: Tapered modification 2 of LMH46-5-X00

Compared to the 'maximum-yield geometry', the chord distribution for *C-20* is reduced with 9.9% at the rotor centre and with 27.5% at the tip. The chord distribution of the root area is the same as for the LMH46-5-X00 rotor blade. Finally the total blade surface is 0.25% larger as for the baseline *C-00* while the radius-weighted blade surface is 0.55% smaller.

2.5 Configurations with the LMH46-5-X60 Blade Geometry

For the configurations described in this section, the airfoil coefficients are calculated for a Reynolds number of $7 \cdot 10^6$. Configuration *C-22* has the blade geometry of the baseline configuration and is added to allow evaluation of the LMH46-5-X60 rotor blade.

Only for configuration C-21 and C-22 the dynamic load set is calculated.

C-21: LMH46-5-X60 rotor blade

On basis of draft results of this parameter sensitivity study, LM Glasfiber already decided to use the tapered configuration *C-20* as basis for their blade geometry. The twist distribution of this geometry was *not optimised* but chosen by LM while also the chord distribution near the tip and near the root were slightly modified. The pre-bend of the blade is modelled similar as for configuration *C-26*.

C-22: LMH46-5-X00, with airfoil coefficients for Re= $7 \cdot 10^6$

Configuration C-21 differs from the baseline configuration C-00 on blade chord distribution, modelling of pre-bent and last but not least, on the fact that airfoil coefficients are used for another Reynolds number. To allow a clear evaluation of the LMH46-5-X60 rotor blade compared to the LMH46-5-X00 rotor blade, the latter is analysed as configuration C-22 with modelling of pre-bent and with airfoils for Re=7·10⁶. The twist is that of configuration C-00, so *not optimised*.

C-23: LMH46-5-X60, with DU 96-W-180 airfoils at the tip

This configuration is similar to configuration C-21 but has DU 96-W-180 airfoils instead of the NACA64-618 airfoils at the tip, both prepared for a Reynolds number $6 \cdot 10^6$.

C-24: LMH46-5-X60, with optimised twist

This configuration is similar to C-21 but has an optimised twist. The optimisation was first done with BOT and later with PHATAS, leading to a similar twist and marginal differences in yield.

2.6 Differences in Structural Aspects

C-25: LMH46-5-X00, no pre-bending

Configuration C-25 with straight blades gives information on the influence of the pre-bend and can also be used as reference to evaluate the detailed modelling of the pre-bend geometry of configuration C-26.

C-26: LMH46-5-X00, with model for pre-bending

For the former configurations the pre-bend of the blades is modelled approximately by using a -1.1deg (upwind) cone angle. For this cone angle the flap moments at the root from centrifugal loads are the same as for the real pre-bend geometry of the LMH46-5-X00 blades.

PHATAS has an option to describe the pre-bend as a curvature. For this option a load set is calculated in which the tip is modelled 2.0m upwind with a local curvature at L=19.9m (R=21.4m). The aim is to compare different ways of modelling the pre-bend shape, also with e.g. FLEX-5.

C-27: LMH46-5-X00, increased damping for tower bending 4%

The tower damping of the NM3000 turbine has a logarithmic decrement of 2% which is a dimensionless damping coefficient of 0.3183%. Compared to the baseline, configuration *C-27* has an increased tower damping of 4%, which is a logarithmic decrement of 25.13%. This can be realised by e.g. installing a water basin inside the tower.

C-28: LMH46-5-X00, modelling of shaft torsion

Modelling shaft torsional deformation will directly influence the in-plane rotor blade motion and the drive train dynamics. In the configurations of the parameter sensitivity study presented here the shaft torsional deformation is *not* modelled because for a realistic response it is necessary to include also the sources of damping in the drive train. In configuration *C-28* shaft torsion is modelled as degree of freedom just for an indication of its influence.

2.7 Influence of Off-shore Locations

C-29: LMH46-5-X00, low "SEA" turbulence

For offshore "SEA" locations the turbulence level is lower except for the very high wind speeds where the wave height has influence on the atmospheric flow. Configuration *C-29* is a preliminary investigation into the influence of the sea climate which will later include wake-operation.

The turbulence intensity at sea is generally smaller because there are no obstacles. For the stronger wind speeds this turbulence intensity increases slightly due to the presence of waves.

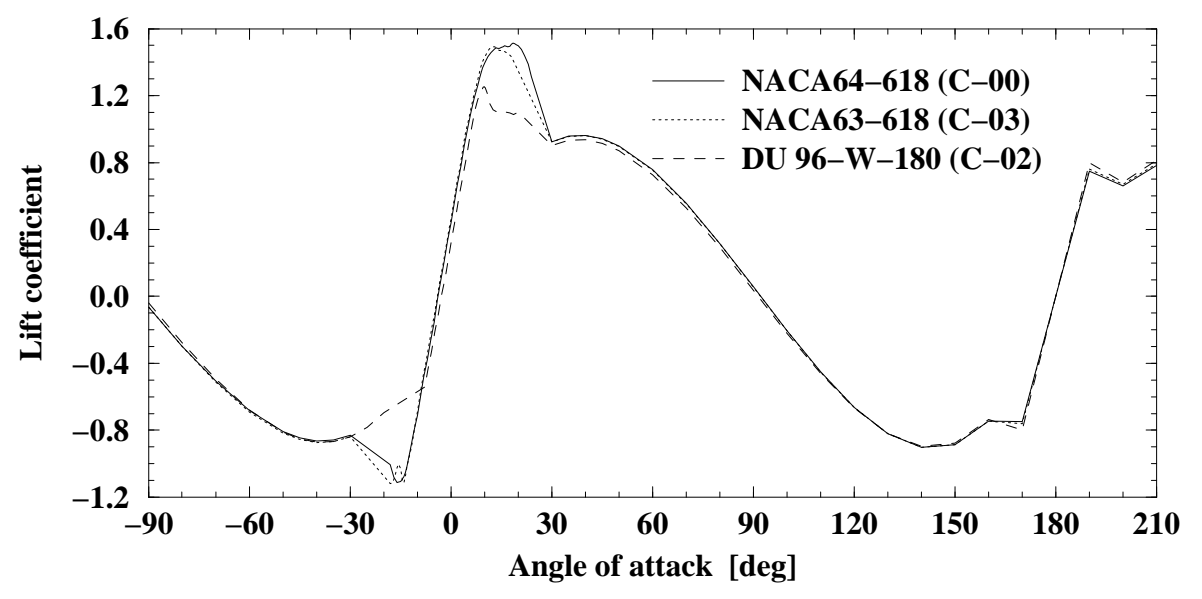


Figure 2.1 Lift coefficients for the outer airfoils

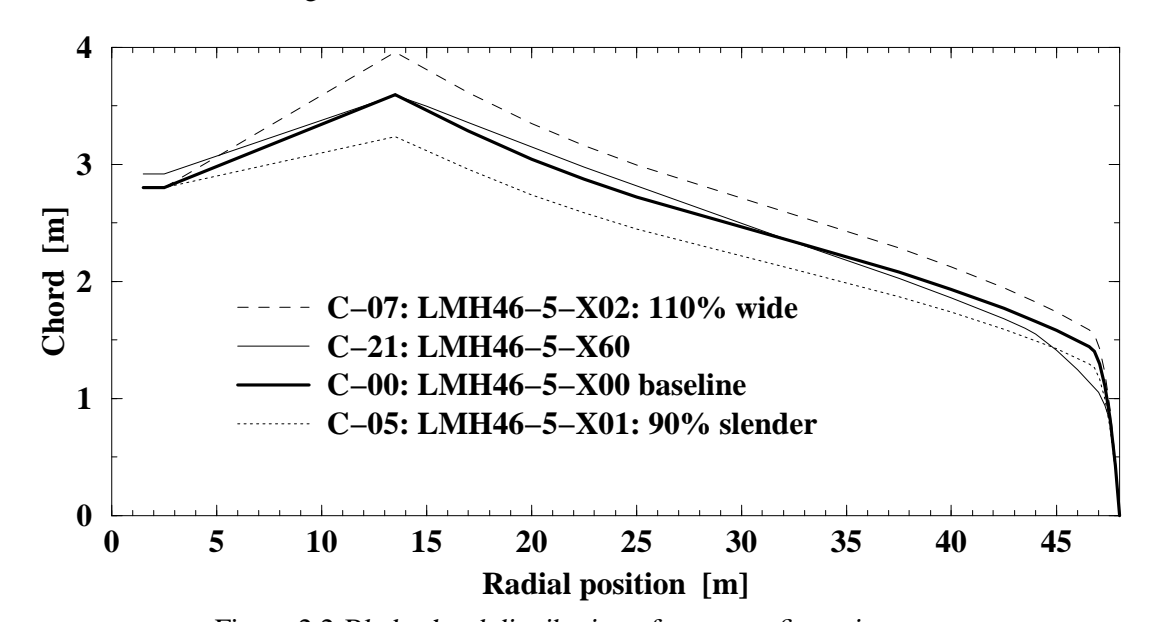


Figure 2.2 Blade chord distribution of some configurations

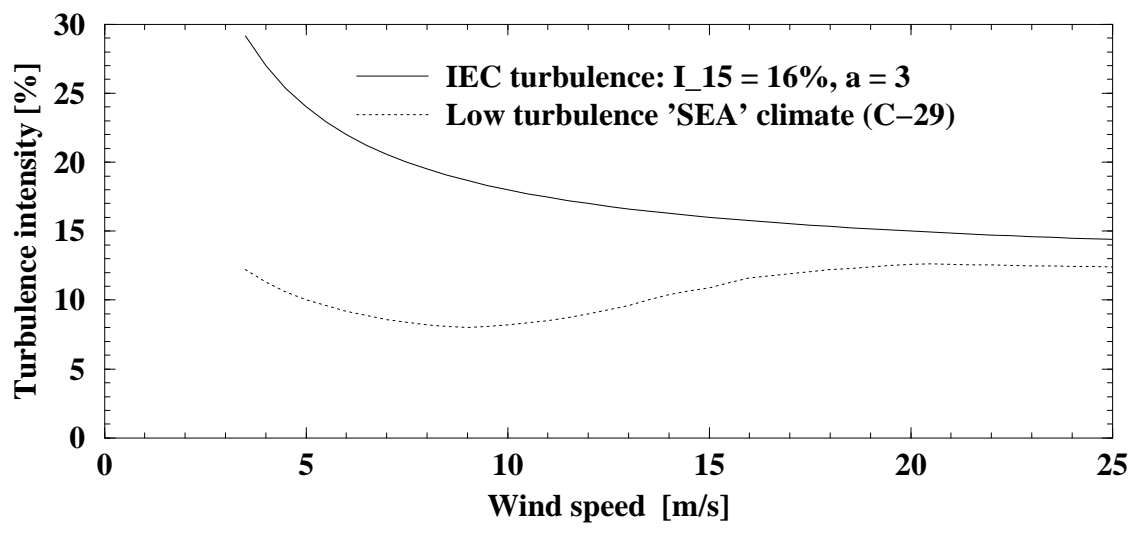


Figure 2.3 Turbulence intensity following IEC and "SEA" climate

3. WIND TURBINE SETTINGS

Because all variations deal with aerodynamic parameters, most of them have consequences for the optimum turbine settings. For a fair comparison the settings of the generator and control algorithm are given the best values on a similar way as done for the baseline configuration, see [13].

3.1 Controller Settings

Thanks to the work of Eric van der Hooft [8], the pitch control algorithm is written in a file that can be used for all configurations which guarantees that the same control concept is used for each load set calculation. The controller settings are stored in an include file datblok3.fi that can be updated for the different aerodynamic concepts.

For configuration *C-02* and *C-03* in which the NACA64-618 airfoils are replaced by DU 96-W-180 and NACA63-618 airfoils respectively (both 18% thick) the differences in aerodynamic rotor characteristics are assumed to be small except in stall. Because the turbine is pitch-controlled towards vane and the controller is only effective above nominal load it was concluded that for the controller the influence from airfoil coefficients is small. For this reason the dynamic loads for these configurations are calculated with the controller settings for the baseline *C-00* configuration. The same is done for the tapered modifications *C-19* and *C-20* and finally for the configurations *C-21* to *C-24* with the LMH46-5-X60 blades.

For the analyses of the configurations with different aspect ratio or with different rotor speed (*C-05* to *C-18*) the controller parameters are adjusted. For the configurations with different airfoil characteristics, the controller settings for the baseline configuration *C-00* are used.

3.2 Partial Load Settings

The partial load generator characteristics and pitch angle settings are chosen for the maximum 'quasi-stationary' energy capture. For most cases however, the partial load generator torque was limited by a lower bound such that the tip-speed ratio in partial load doesn't exceed $\lambda=7.5$. For the load sets with reduced rotor speed (86.6%, 90.3% and 93.3%) the tip speed ratio in partial load was consequently maximised to 6.50, 6.77 and 7.00 respectively.

The "quasi-stationary" annual energy capture was calculated with almost the same aerodynamic and structural dynamic modelling as for the calculation of the dynamic loads. The differences are: **Turbulence Intensity** For the annual energy yield the turbulence intensity (at 15m/s) is 12% while for the structural loads the turbulence intensity is 16%.

Misalignment: Odeg For the quasi-stationary energy capture both the misalignment and the upflow of the wind are zero.

Vertical Shear: 0.16 For the IEC load calculations the vertical shear follows a power law with an exponent of 0.2. Knowing that in general the criteria are according to conservative guidelines and knowing that the Germanischer Lloyd rules and regulations [6] prescribe a power law with exponent 0.16, the latter value is used to calculate the quasi-stationary energy capture.

Pitch Error: 0.3deg The dynamic loads are calculated with a pitch error of blade 2 and 3 of +0.5deg and -0.5deg respectively. Based on the assumption that these values are meant to analyse the worst loads, the average pitch error is assumed to be +0.3deg and -0.3deg respectively.

Tip Loss: R-0.5m The LMH46-5 rotor blades have a reversed twist over the outer 4m of the span such that the tip vortex is distributed. The aim of this twist is to reduce the aerodynamic noise, although it also gives a smaller radius of the 'effective tip-trailing vorticity'. For the LMH46-5-X00 rotor blade operating at a pitch angle of 0.0deg and a tip speed ratio of 7.5 the

calculated location of this 'effective tip-trailing vorticity' is at a radius 1.03m smaller than the rotor radius. If the outer part of the blade is tapered linearly towards the tip, with a chord of 1.4m and zero tip-twist (for conventional blades), the effective tip-trailing vorticity is 0.55m more inboard of the rotor radius. Compared to the tip radius for a tapered blade, the radius of the tip vorticity of the aero-acoustic shaped tip is 0.5m smaller. This 0.5m smaller radius is used in the expression for the tip-loss factor of Prandtl when calculating the 'quasi-stationary' annual energy capture. Based on the design-aim of the aero-acoustic shaped tip to distribute the tip trailing vorticity over a certain span, this 0.5m smaller 'tip-vortex radius' is applied for all configurations. For the calculation of the dynamic loads, the tip loss factor is calculated with the real rotor radius because the reverse-twisted tip is still sensitive to gusts and turbulence.

In partial load the rotor is operating at optimum lambda, which is characterised by a quadratic relation between torque and rotor speed. The aerodynamic torque (and thus the generator torque) for each of the blade configurations may be different. With the program PHATAS the level of the partial load generator torque is adjusted such that the optimum lambda characteristics is obtained, while the tip speed ratio does not exceed 7.5, except for configuration *C-17* and *C-18*.

	Chord		Partial load settings		Nominal
	w.r.t. max	Control	Generator	Pitch	shaft
Configuration	yield	settings	torque	angle	torque
C-00: LMH46-5-X00 "baseline"	78.34%	C-00	66.0%	0.0deg	100%
C-01: X00, Former baseline, n.o.t.	78.34%	C-01	65.4%	$0.4 \deg$	+0%
C-02: X03: DU 96-W-180 airfoil	78.3%	C-00	65.4%	-0.8deg	+0%
C-03: X00, with NACA63-618 airfoil	78.3%	C-00	65.6%	$0.2 \deg$	+0%
C-04: 80% slender chord	62.67%	C-05	63.9%	-0.5deg	+0%
C-05, C-06: X01: 90% slender chord	70.51%	C-05	65.2%	$0.8 \deg$	+0%
C-07, C-08: X02: 110% wide chord	86.12%	C-07	66.0%	1.1deg	+0%
C-09: 120% wide chord	94.01%	C-07	66.0%	0.9deg	+0%
C-10: X00, 86.6% speed, n.o.t.	58.75%	C-10	63.4%	0.1deg	+15.47%
C-11: X00, 86.6% sub-optimal speed	58.75%	C-10	63.4%	-0.9deg	+15.47%
C-12: X00, 90.3% speed, n.o.t.	63.88%	C-12	64.7%	$0.0 \deg$	+10.74%
C-13: X00, 90.3% sub-optimal speed	63.88%	C-12	64.7%	-0.3deg	+10.74%
C-14: X00, 93.3% speed, n.o.t.	68.20%	C-12+	65.2%	$0.4 \deg$	+7.18%
C-15: X00, 93.3% sub-optimal speed	68.20%	C-12+	65.3%	$0.7 \deg$	+7.18%
C-16: X00, Maximum tip speed 80m/s	89.14%	C-00+	80.0%	$0.2 \deg$	-6.25%
C-17: Tip speed 79m/s, 95% chord	82.58%	C-00+	66.9%	$0.2 \deg$	-5.0%
C-18: Tip speed 79m/s, 90% chord	78.23%	C-18	68.5%	-0.1deg	-5.0%
C-19: Tapered modification 1 of X00	78.13%	C-00	65.8%	0.3deg	+0%
C-20: Tapered modification 2 of X00	77.91%	C-00	65.8%	$0.5 \deg$	+0%
C-21: LMH46-5-X60 , Re= $7 \cdot 10^6$, n.o.t.	77.4%	C-00	66.9%	0.4deg	+0%
C-22: LMH46-5-X00, Re= $7 \cdot 10^6$, n.o.t.	78.3%	C-00	67.5%	$0.0 \deg$	+0%
C-23: X60, DU 96-W-180 airfoil, n.o.t.	77.4%	C-00	66.4%	-0.4deg	+0%
C-24: X60, with optimised twist	77.4%	C-00	67.3%	-0.5deg	+0%
C-25: X00, no pre-bending	78.34%	C-00	65.7%	0.1deg	+0%
C-26: X00, with model for pre-bend	78.34%	C-00	66.0%	$0.0 \deg$	+0%
C-27: X00, 4% tower damping	78.34%	C-00	66.0%	$0.0 \deg$	+0%
C-28: X00, modelling shaft torsion	78.34%	C-00	66.0%	$0.0 \deg$	+0%
C-29: X00, low turbulence: "SEA"	78.34%	C-00	66.0%	0.3deg	+0%

Here 'n.o.t.' stands for non-optimised twist. A control algorithm *C-00+* indicates a modified *C-00* controller. The 'Partial load Generator torque' is expressed with respect to the nominal torque at nominal speed for a power of 3 MW. For the tapered configurations the 'chord w.r.t. max yield' is calculated with the spanwise integral of the radius-weighted chord distribution.

4. COMPARISON

4.1 Calculated Power Production

With the Blade Optimisation Tool BOT the rotor is modelled flat and perpendicular to the wind and has a uniform wind loading over the rotor plane. In BOT the structural dynamics are not included while stationary airfoil coefficients are used. Generator characteristics can be included as function of wind speed.

In the power curve calculation with PHATAS the influence of the control algorithm but also of all structural and aerodynamic aspects are included. The annual energy capture can be integrated directly from the stationary power curve or after adding the energy that is present in the turbulence, of which the results are listed in column 3 and 4 of the following table.

Configuration	From BOT	Stationary	Turbulent	Dynamic
C-00: LMH46-5-X00 "baseline"	100%	100%	100%	100%
C-01: X00, Former baseline, n.o.t.	-0.233%	-0.37%	-0.27%	-0.29%
C-02: X03: DU 96-W-180 airfoil	-0.023%	-0.19%	-0.16%	-0.37%
C-03: X00, with NACA63-618 airfoil	-0.023%	-0.08%	-0.02%	not
C-04: 80% slender chord	-1.928%	-2.82%	-3.59%	not
C-05: X01: 90% slender chord	-0.739%	-1.07%	-1.44%	-2.09%
C-06: X01: 90% chord, 81% stiffn.	-0.739%	-1.28%	-1.72%	-2.08%
C-07: X02: 110% wide chord	+0.241%	+0.17%	+0.32%	+0.79%
C-08: X02: 110% chord, 121% stiffn.	+0.241%	+0.38%	+0.53%	+0.73%
C-09: 120% wide chord	+0.342%	+0.27%	+0.57%	not
C-10: X00, 86.6% speed, n.o.t.	-4.238%	-5.20%	-5.76%	-7.16%
C-11: X00, 86.6% sub-optimal speed	-2.745%	-3.44%	-4.33%	-5.96%
C-12: X00, 90.3% speed, n.o.t.	-2.216%	-2.58%	-3.49%	-3.98%
C-13: X00, 90.3% sub-optimal speed	-1.578%	-1.77%	-2.44%	-4.05%
C-14: X00, 93.3% speed, n.o.t.	-0.972%	-1.18%	-1.78%	not
C-15: X00, 93.3% sub-optimal speed	-0.925%	-1.08%	-1.64%	-3.11%
C-16: X00, Maximum tip speed 80m/s	+0.381%	-0.10%	+0.53%	not
C-17: Tip speed 79m/s, 95% chord	+0.365%	+0.16%	+0.23%	+0.38%
C-18: Tip speed 79m/s, 90% chord	+0.140%	-0.49%	+0.14%	-0.71%
C-19: Tapered modification 1 of X00	-0.008%	-0.08%	-0.07%	-0.12%
C-20: Tapered modification 2 of X00	-0.016%	-0.10%	+0.01%	-0.14%
C-21: LMH46-5-X60 , Re= $7 \cdot 10^6$, n.o.t.	+0.428%	+0.50%	+0.52%	-0.23%
C-22: LMH46-5-X00, Re= $7 \cdot 10^6$, n.o.t.	+0.490%	+1.13%	+1.18%	+0.57%
C-23: X60, DU 96-W-180 airfoil, n.o.t.	+0.156%	+0.36%	+0.40%	not
C-24: X60, with optimised twist	+0.669%	+0.71%	+0.71%	not
C-25: X00, no pre-bending	+0.0%	-0.34%	-0.21%	+0.03%
C-26: X00, with model for pre-bend	+0.0%	+0.73%	+0.70%	-0.05%
C-27: X00, 4% tower damping	+0.0%	-0.00%	-0.01%	+0.00%
C-28: X00, modelling shaft torsion	+0.0%	-0.00%	-0.02%	-0.08%
C-29: X00, low turbulence: "SEA"	+0.0%	+0.00%	-0.86%	-1.58%

In this table the power production is calculated in different ways:

Production from BOT In BOT only the aerodynamic characteristics of the rotor are modelled without the presence of the tower while the geometry does not include the tilt angle.

The cone angle of the rotor is not described, although this is negligible for the NM3000 turbine. The wind loading is constant and uniform over the rotor plane.

Stationary production The stationary production is calculated with PHATAS in which the generator curve and the pitch control are included. All aerodynamic and structural dynamic properties

of the turbine are modelled. The wind loading is stationary for each wind speed value and has a power law for the vertical shear with an exponent 0.16. The annual yield is integrated from the resulting P-V table.

Turbulent production The turbulence that is present in the wind also contains energy while variations in wind velocity may give a loss of energy if the control algorithm reacts not fast enough. An analytical expression for the average power in turbulent wind is given by Rosen and Sheinmann [14] as: $P_{\text{turb}} = P_{\text{stat}} \left(1 + 3 I_{\text{V}}^2 \delta_{\text{V}} \right)$

with
$$\delta_{
m V}=1+\left(\,\partial C_{
m P}/\partial \,V+\left(\partial^2 \,C_{
m P}/\partial \,V^2
ight)\,V/6\,
ight)\,V/C_{
m P}$$
 .

The expression for δ_V contains the second wind-speed derivative of the turbine power. Around nominal wind speed this second derivative will have strong negative values.

Around and above nominal wind speed the NM3000 turbine allows rotor-speed variations (limited by the controller to 17.6rpm) which has the effect that fluctuations in wind energy from turbulence can be buffered in rotational energy of the rotor. Because of this so-called "fly-wheel effect" the loss of energy due to wind fluctuations is limited. Based on investigations by T.G. van Engelen and E.L. van der Hooft for the NM3000 controller in turbulent wind the so-called efficiency of the turbine-controller around nominal power is established at 96% which means that $P_{\rm turb}$ is always at least 0.96 $P_{\rm stat}$. The **Turbulent production** is calculated with this efficiency. At rotor speed values where the generator characteristics have discontinuities, the turbulent power shows to be smaller than the stationary power because at these points the second derivative of the power coefficient is negative.

Dynamic production The dynamic power production is calculated from the production load cases of the IEC load set. The resulting power curve contains all dynamics of the turbine and the wind that are modelled in PHATAS. Because the IEC load set is meant to obtain the design loads, it has some conservatism: • The vertical shear exponent is 0.2 (instead of 0.16); • The pitch error of the blades is 0.5deg (instead of 0.3deg); • The yaw misalignment is +10deg or -10deg; • The turbulence intensity (at 15m/s) is 16% (instead of 12%).

The wind turbine settings listed in chapter 3 are those giving the largest "Turbulent" production within the tip-speed-ratio limitation. The "Quasi stationary" energy production for the SEA cli-

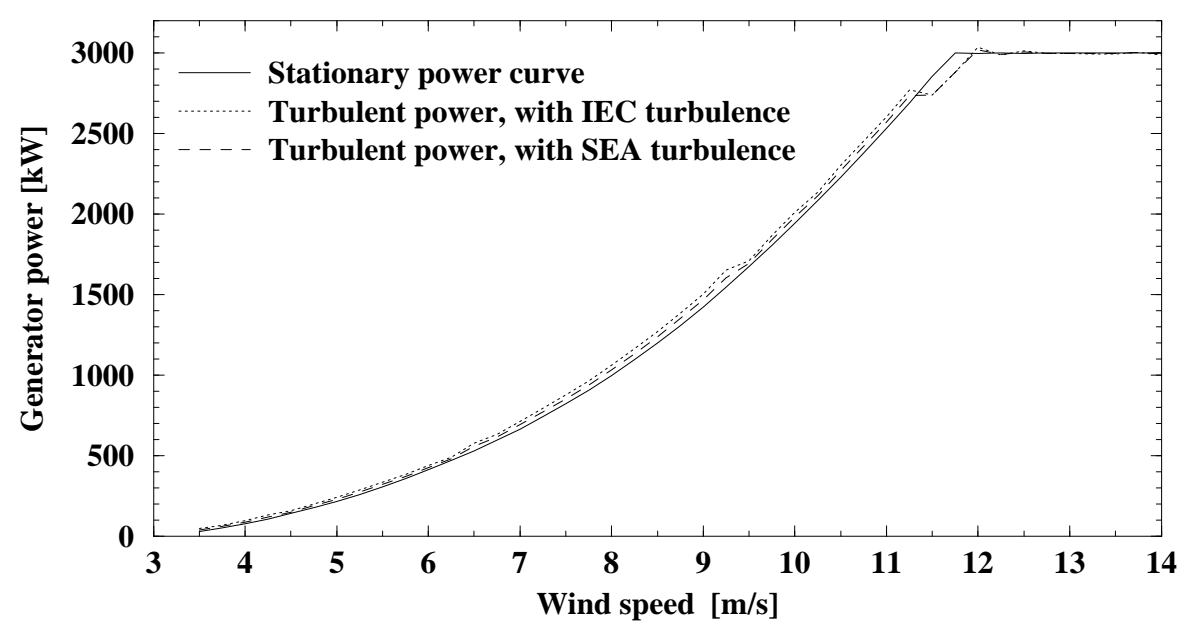


Figure 4.1 Stationary and turbulent power curves

mate is calculated with a constant turbulence intensity of 9%, (12% for the other configurations). For configuration *C-29* with low turbulence one would expect less loss of energy from the time delay between controller actions and wind speed fluctuations and less loss of energy for variations

around nominal power. Nevertheless the energy capture from the dynamic load time series is smaller than for the IEC wind loading (configuration C-00) which is caused by the simple fact that also the wind turbulence contains energy. Figure 4.2 shows the annual energy capture of the configurations as calculated from the dynamic load set. In figure 4.3 the calculated annual

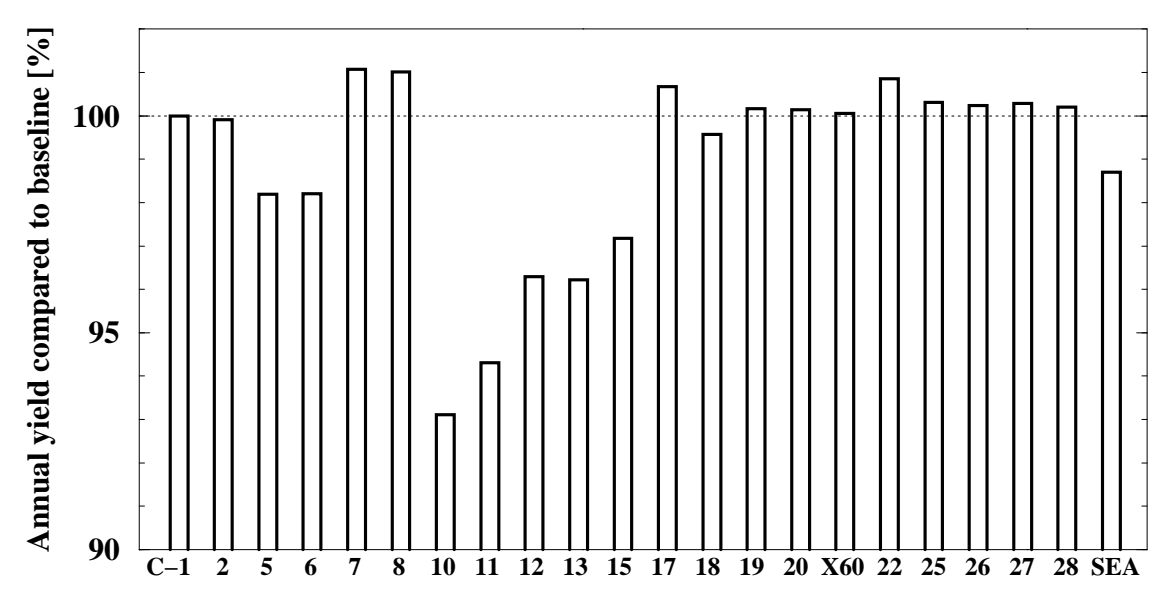


Figure 4.2 Energy capture calculated from the dynamic load set

energy capture is plotted versus the 'effective solidity' which is the product of chord and nominal speed squared. In figure 4.3 all values are made dimensionless by dividing through value for the baseline. In this plot, only the configurations with the airfoils as for the baseline configuration are used. The geometry for which the program BOT gives a maximum energy capture will have an 'effective solidity' of 127.6% compared to the baseline. This figure shows clearly that the annual

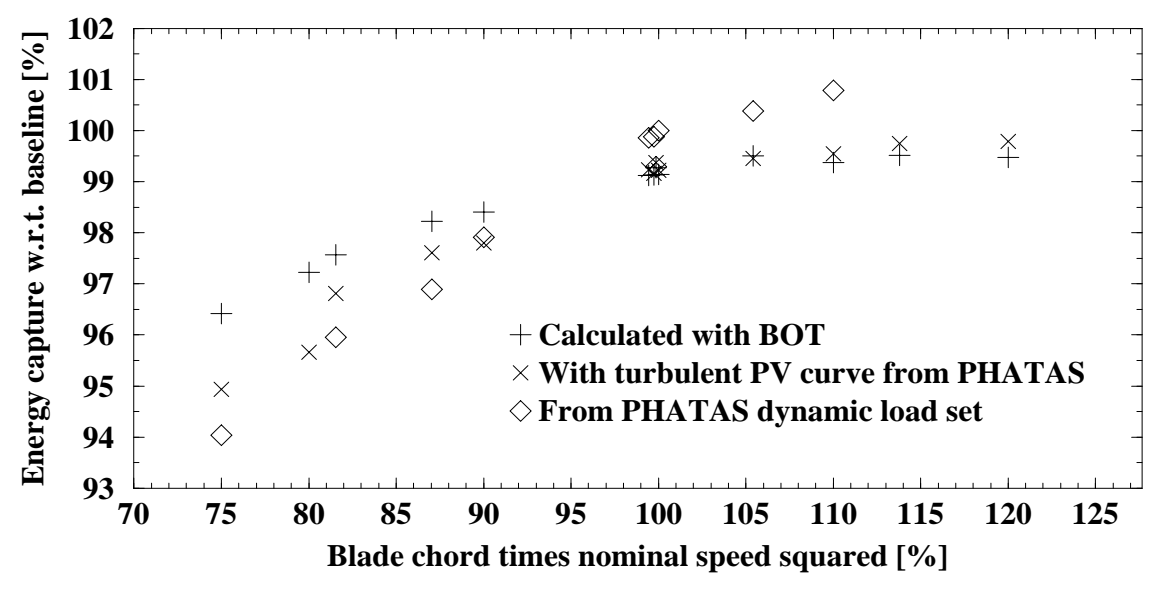


Figure 4.3 Energy capture as function of effective solidity

energy capture is a quadratic function of the blade chord, both when calculated with BOT and with PHATAS. From the energy capture calculated with PHATAS one may conclude that the chord for maximum energy capture is larger than if calculated with BOT. A possible reason may be found in the progressive increase of the drag coefficient with angle of attack. For this reason the average drag coefficient in turbulent wind is larger than the drag coefficient at the average angle of attack. For a blade with a smaller chord, this progressive character of the drag coefficient gives a stronger

loss of annual energy yield. This means that the chord for maximum yield in turbulent wind may be somewhat larger than that in constant wind.

Another explanation may be that in BOT (in order to reduce CPU time) the generator characteristics are modelled as a simple function of wind speed, instead of rotor speed.

4.2 Extreme Loads

4.2.1 Extreme rotor speed

Since the pitch control algorithm intends to keep the rotor-speed between limits, the maximum overall rotor speed and the maximum rotor speed during production is listed here.

	Overall	Load	Production	Load	Fatigue
Configuration	speed	case	speed	case	average
C-00: LMH46-5-X00 "baseline"	100%	162	100%	120	11.380
C-01: X00, Former baseline, n.o.t.	-0.69%	157	+0.20%	123	11.402
C-02: X03: DU 96-W-180 airfoil	+0.32%	162	-0.05%	120	11.367
C-05: X01: 90% slender chord	-0.69%	162	+0.20%	123	11.346
C-06: X01: 90% chord, 81% stiffn.	-0.22%	162	-0.04%	122	11.347
C-07: X02: 110% wide chord	+4.75%	162	+0.52%	123	11.423
C-08: X02: 110% chord, 121% stiffn.	-0.94%	162	+0.07%	123	11.423
C-10: X00, 86.6% speed, n.o.t.	-11.32%	191	-10.47%	123	9.721
C-11: X00, 86.6% sub-optimal speed	-11.84%	162	-10.70%	123	9.754
C-12: X00, 90.3% speed, n.o.t.	-7.96%	162	-8.67%	123	10.221
C-13: X00, 90.3% sub-optimal speed	-6.16%	162	-8.48%	123	10.208
C-15: X00, 93.3% sub-optimal speed	-1.70%	191	-5.64%	123	10.585
C-17: Tip speed 79m/s, 95% chord	+4.95%	162	+3.72%	123	11.896
C-18: Tip speed 79m/s, 90% chord	+5.13%	162	+3.87%	124	11.956
C-19: Tapered modification 1 of X00	+0.92%	162	+0.15%	124	11.391
C-20: Tapered modification 2 of X00	+0.68%	162	-0.43%	123	11.391
C-21: LMH46-5-X60 , Re= $7 \cdot 10^6$, n.o.t.	+0.92%	162	+0.80%	122	11.394
C-22: LMH46-5-X00, Re= $7 \cdot 10^6$, n.o.t.	+1.21%	162	+0.26%	122	11.398
C-25: X00, no pre-bending	+0.33%	162	+0.46%	122	11.392
C-26: X00, with model for pre-bend	+0.48%	162	-0.46%	124	11.387
C-27: X00, 4% tower damping	+0.56%	162	-0.19%	120	11.391
C-28: X00, modelling shaft torsion	+0.78%	162	+0.20%	117	11.386
C-29: X00, low turbulence: "SEA"	+0.00%	162	-1.16%	122	11.343

The last column contains the average rotor speed from the calculated fatigue load spectrum for a Weibull wind distribution with an average of 9m/s.

Over a period of 20 years an average rotor speed of e.g. 11.4rpm gives about 120 10⁶ revolutions. Here the average rotor speed is not directly related to the operating speed because the generator characteristics of the configurations may differ.

4.2.2 Extreme tower base moments

The extreme moments calculated for the tower base are listed in the following table.

	Production Load		Overall	Load	Including
Configuration	moment	case	excl. ice	case	ice (811)
C-00: LMH46-5-X00 "baseline"	100%	124	100%	157	<
C-01: X00, Former baseline, n.o.t.	+1.64%	123	-12.06%	511	<
C-02: X03: DU 96-W-180 airfoil	-10.91%	123	-14.04%	157	<
C-05: X01: 90% slender chord	-4.19%	123	-5.43%	158	<
C-06: X01: 90% chord, 81% stiffn.	+0.22%	123	-5.20%	158	<
C-07: X02: 110% wide chord	+14.11%	122	-2.24%	157	<
C-08: X02: 110% chord, 121% stiffn.	+9.93%	124	+4.91%	611	<
C-10: X00, 86.6% speed, n.o.t.	-12.30%	123	-13.21%	158	+83.04%
C-11: X00, 86.6% sub-optimal speed	-7.02%	123	-9.42%	157	+64.08%
C-12: X00, 90.3% speed, n.o.t.	-5.46%	124	-10.55%	157	+18.20%
C-13: X00, 90.3% sub-optimal speed	+0.18%	124	-8.95%	157	+11.33%
C-15: X00, 93.3% sub-optimal speed	+0.83%	124	+18.53%	611	<
C-17: Tip speed 79m/s, 95% chord	+1.74%	117	+6.56%	157	<
C-18: Tip speed 79m/s, 90% chord	+6.41%	123	+4.34%	157	<
C-19: Tapered modification 1 of X00	+0.37%	123	+0.17%	157	<
C-20: Tapered modification 2 of X00	+3.41%	124	+0.52%	157	<
C-21: LMH46-5-X60 , Re= $7 \cdot 10^6$, n.o.t.	+1.68%	124	+2.55%	157	<
C-22: LMH46-5-X00, Re= $7 \cdot 10^6$, n.o.t.	+1.36%	124	+1.62%	157	<
C-25: X00, no pre-bending	+0.86%	124	+0.14%	157	<
C-26: X00, with model for pre-bend	+1.26%	123	-0.15%	157	<
C-27: X00, 4% tower damping	-12.21%	117	-9.30%	157	<
C-28: X00, modelling shaft torsion	+6.00%	124	+0.04%	157	<
C-29: X00, low turbulence: "SEA"	-3.54%	124	+0.0%	157	<

In this table <— indicates that even with 'ice load cases' the extreme values are the same as without ice. The large extreme tower base moments for the "86.6% reduced rotor speed" configu-

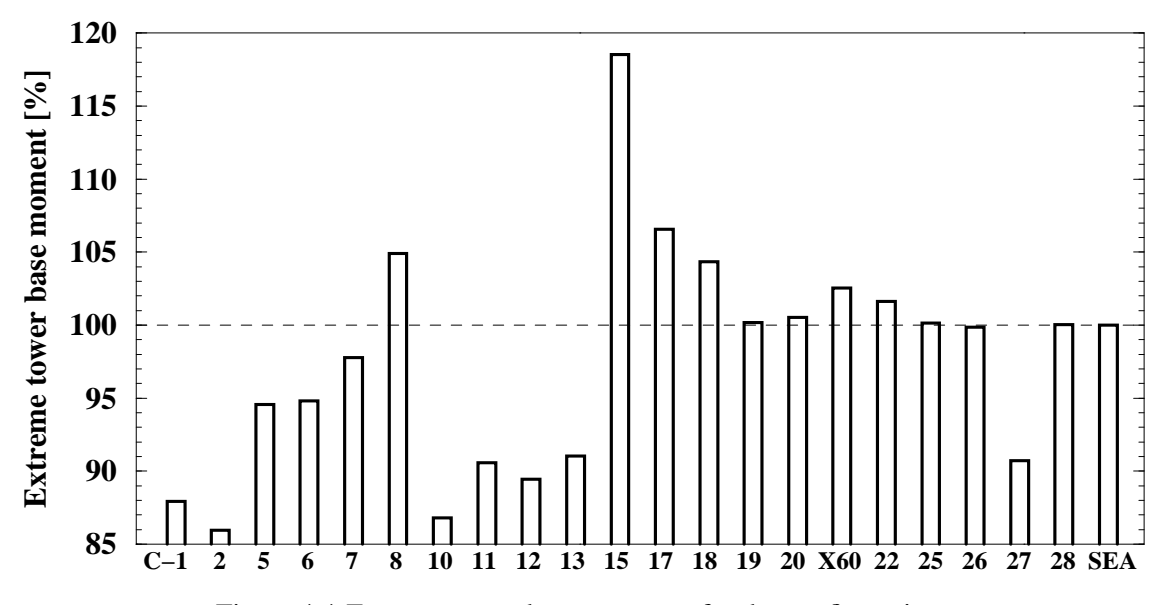


Figure 4.4 Extreme tower base moments for the configurations

rations with ice on two blades (load case file 811) are probably the result of resonances. For this configuration the second extreme tower base moment is 13.21% smaller than the extreme for the baseline *C-00* and is found in load case file 158 while the third extreme moment is found in load case file 157 and is 13.225% smaller (not in the table).

The graphs with dynamic load time series of load-case file 811 for the 86.6% sub-optimal speed configuration *C-10* shows large 0.2Hz fluctuations in rotor speed and power. This together with the fact that the extreme side moment in the tower base is 2.3 times larger than the extreme fore-aft moment is indicative of sideways vibrations of the turbine. Because the calculations performed here are in the pre-design stage, the tower frequencies of the final design are probably different. In order to avoid large excessive loads from tower vibration, large wind turbines will probably have a vibration sensor in the nacelle for which it is not realistic to compare configurations on basis of load-cases with blade-icing.

Therefore the overall extreme loads including ice, and their load-case file, are listed separately in the rightmost columns of the table.

A calculation is performed for this 86.6% sub-optimal speed configuration *C-10* in which the shaft torsional flexibility is modelled. The extreme tower base moment for the load case with ice on 2 blades (file 811) is 81.6% higher than for the baseline configuration, which gives a 2% reduction compared to a rigid shaft. The smaller coupling between tower bending and drive train dynamics for a flexible shaft may be the reason for the smaller dynamic response.

4.2.3 Extreme tower top moments

The extreme moments calculated for the tower top are listed in the following table.

	Production	n Load	Overall	Load	Including	Load
Configuration	moment	case	excl. ice	case	ice	case
C-00: LMH46-5-X00 "baseline"	100%	124	100%	162	<	
C-01: X00, Former baseline, n.o.t.	-5.00%	124	+5.03%	162	<	
C-02: X03: DU 96-W-180 airfoil	-2.65%	124	-15.00%	132	<	
C-05: X01: 90% slender chord	+1.13%	124	+3.24%	162	<	
C-06: X01: 90% chord, 81% stiffn.	+2.53%	124	+3.19%	162	<	
C-07: X02: 110% wide chord	-2.28%	124	+6.62%	157	<	
C-08: X02: 110% chord, 121% stiffn.	+4.88%	122	+4.06%	162	+8.04%	821
C-10: X00, 86.6% speed, n.o.t.	-8.88%	124	-9.52%	162	-6.24%	811
C-11: X00, 86.6% sub-optimal speed	-6.15%	124	-6.36%	162	<	
C-12: X00, 90.3% speed, n.o.t.	-10.93%	124	-2.23%	162	<	
C-13: X00, 90.3% sub-optimal speed	-3.84%	124	+0.73%	162	<	
C-15: X00, 93.3% sub-optimal speed	+2.22%	124	+9.05%	162	<	
C-17: Tip speed 79m/s, 95% chord	+3.27%	122	+18.23%	162	<	
C-18: Tip speed 79m/s, 90% chord	+3.50%	124	+15.24%	162	<	
C-19: Tapered modification 1 of X00	+4.71%	124	+5.46%	162	<	
C-20: Tapered modification 2 of X00	+0.95%	124	+0.01%	162	<	
<i>C-21</i> : LMH46-5-X60 , Re=7·10 ⁶ , <i>n.o.t.</i>	+6.52%	124	+0.11%	162	<	
C-22: LMH46-5-X00, Re= $7 \cdot 10^6$, n.o.t.	+4.30%	124	+4.34%	162	<	
C-25: X00, no pre-bending	+0.60%	124	+1.12%	162	<	
C-26: X00, with model for pre-bend	+5.05%	124	+0.37%	162	<	
C-27: X00, 4% tower damping	+5.59%	124	-4.37%	162	<	
C-28: X00, modelling shaft torsion	+9.60%	124	+1.04%	162	<	
C-29: X00, low turbulence: "SEA"	-0.67%	124	+0.00%	162	<	

The relatively large tower top loads for configuration C-21 with LMH46-5-X60 rotor blades are mainly a result of the larger aerodynamic coefficients for a Reynolds number of $7 \cdot 10^6$.

4.2.4 Extreme shaft moments

The following extreme rotor shaft bending moments are selected 1.8m aft of the rotor centre.

	Production	Load	Overall	Load
Configuration	moment	case	moment	case
C-00: LMH46-5-X00 "baseline"	100%	122	100%	162
C-01: X00, Former baseline, n.o.t.	+5.64%	123	+1.20%	822
C-02: X03: DU 96-W-180 airfoil	-2.51%	124	+9.19%	132
C-05: X01: 90% slender chord	-8.39%	124	-4.98%	162
C-06: X01: 90% chord, 81% stiffn.	-6.76%	124	-1.36%	822
C-07: X02: 110% wide chord	+5.95%	124	+8.72%	212
C-08: X02: 110% chord, 121% stiffn.	+14.30%	124	+12.03%	821
C-10: X00, 86.6% speed, n.o.t.	-10.86%	124	-1.52%	822
C-11: X00, 86.6% sub-optimal speed	-6.42%	124	-7.68%	821
C-12: X00, 90.3% speed, n.o.t.	-4.73%	124	-6.33%	132
C-13: X00, 90.3% sub-optimal speed	-2.62%	122	-2.45%	132
C-15: X00, 93.3% sub-optimal speed	-6.11%	122	+3.78%	822
C-17: Tip speed 79m/s, 95% chord	+10.04%	122	+4.98%	162
C-18: Tip speed 79m/s, 90% chord	+1.35%	124	+2.84%	162
C-19: Tapered modification 1 of X00	-0.36%	124	+0.41%	162
C-20: Tapered modification 2 of X00	-0.66%	123	+0.00%	162
C-21: LMH46-5-X60 , Re= $7 \cdot 10^6$, n.o.t.	+2.94%	124	+0.08%	162
C-22: LMH46-5-X00, Re= $7 \cdot 10^6$, n.o.t.	+2.55%	124	+0.41%	162
C-25: X00, no pre-bending	-3.56%	123	-1.04%	162
C-26: X00, with model for pre-bend	-0.05%	124	-1.93%	162
C-27: X00, 4% tower damping	+6.29%	124	+0.05%	162
C-28: X00, modelling shaft torsion	+11.65%	124	+1.50%	124
C-29: X00, low turbulence: "SEA"	+0.89%	124	+0.00%	162

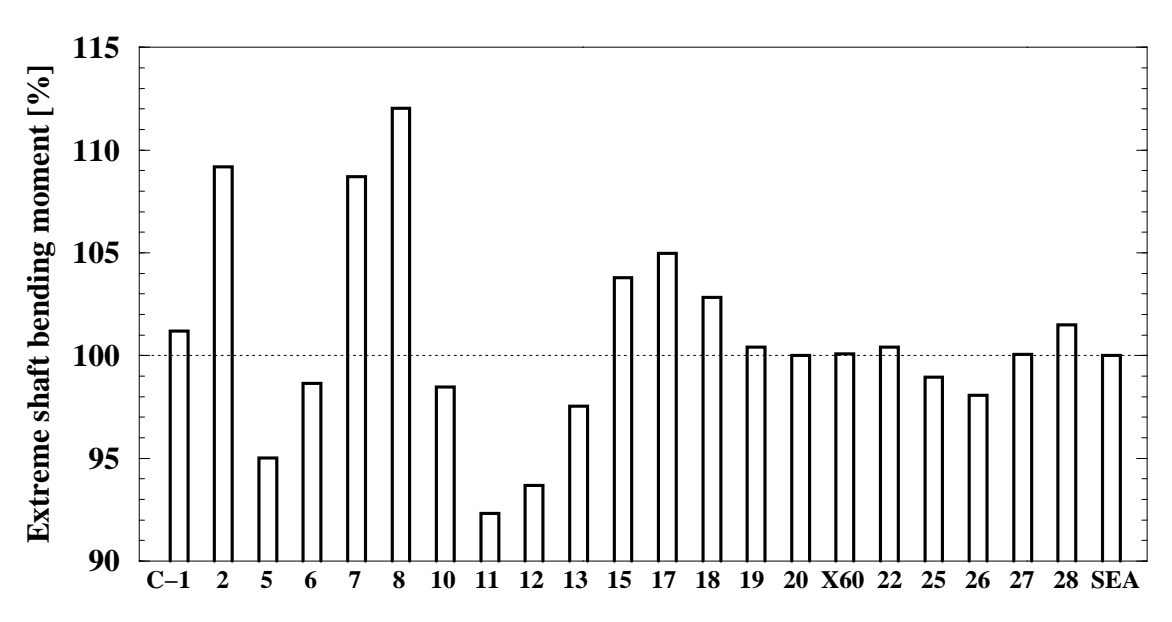


Figure 4.5 Extreme shaft bending moments for the configurations

4.2.5 Extreme blade root moments

The different extreme moments in the blade root connection are listed in the following table.

	Production	n Load	Overall	Load	Except	Load
Configuration	moment	case	moment	case	131, 132	case
C-00: LMH46-5-X00 "baseline"	100%	112	+11.52%	132	100%	161
C-01: X00, Former baseline, n.o.t.	+1.07%	114	+3.71%	131	-0.42%	512
C-02: X03: DU 96-W-180 airfoil	-1.64%	124	+14.73%	131	-3.02%	161
C-05: X01: 90% slender chord	-1.68%	116	+9.60%	131	-6.76%	162
C-06: X01: 90% chord, 81% stiffn.	-6.42%	120	+12.41%	131	-7.15%	162
C-07: X02: 110% wide chord	+7.27%	115	+1.02%	115	+1.02%	115
C-08: X02: 110% chord, 121% stiffn.	+9.44%	115	+6.75%	821	+6.75%	821
C-10: X00, 86.6% speed, n.o.t.	-2.07%	112	+9.29%	131	-2.62%	811
C-11: X00, 86.6% sub-optimal speed	-8.26%	112	+9.94%	131	-7.09%	811
C-12: X00, 90.3% speed, n.o.t.	-5.52%	112	+4.58%	131	-5.41%	812
C-13: X00, 90.3% sub-optimal speed	-4.73%	112	+10.46%	131	-6.32%	811
C-15: X00, 93.3% sub-optimal speed	-3.64%	124	+10.84%	131	-6.04%	811
C-17: Tip speed 79m/s, 95% chord	+0.56%	115	+16.32%	131	+1.57%	162
C-18: Tip speed 79m/s, 90% chord	-4.72%	112	+2.15%	131	-2.44%	162
C-19: Tapered modification 1 of X00	+3.91%	115	+1.75%	131	-0.80%	161
C-20: Tapered modification 2 of X00	-0.47%	112	-0.26%	161	-0.26%	161
C-21: LMH46-5-X60 , Re= $7 \cdot 10^6$, n.o.t.	+4.10%	115	+1.64%	161	+1.64%	161
C-22: LMH46-5-X00, Re= $7 \cdot 10^6$, n.o.t.	+2.07%	124	+2.48%	161	+2.48%	161
C-25: X00, no pre-bending	-2.47%	115	-0.24%	131	-0.83%	157
C-26: X00, with model for pre-bend	+3.15%	124	+16.43%	131	+0.23%	161
C-27: X00, 4% tower damping	+0.23%	112	-0.87%	161	-0.87%	161
C-28: X00, modelling shaft torsion	+2.39%	115	+2.42%	131	+0.04%	161
C-29: X00, low turbulence: "SEA"	-6.20%	112	+11.52%	132	+0.00%	161
The column 'Overall moment' contains di	fforoncoc v	ith room	ot to "the ov	trama n	nomant for	tho

The column 'Overall moment' contains differences with respect to "the extreme moment for the baseline without load case 131 and 132".

The extreme moment for the "wide" configuration C-07 is not so large while it also does not

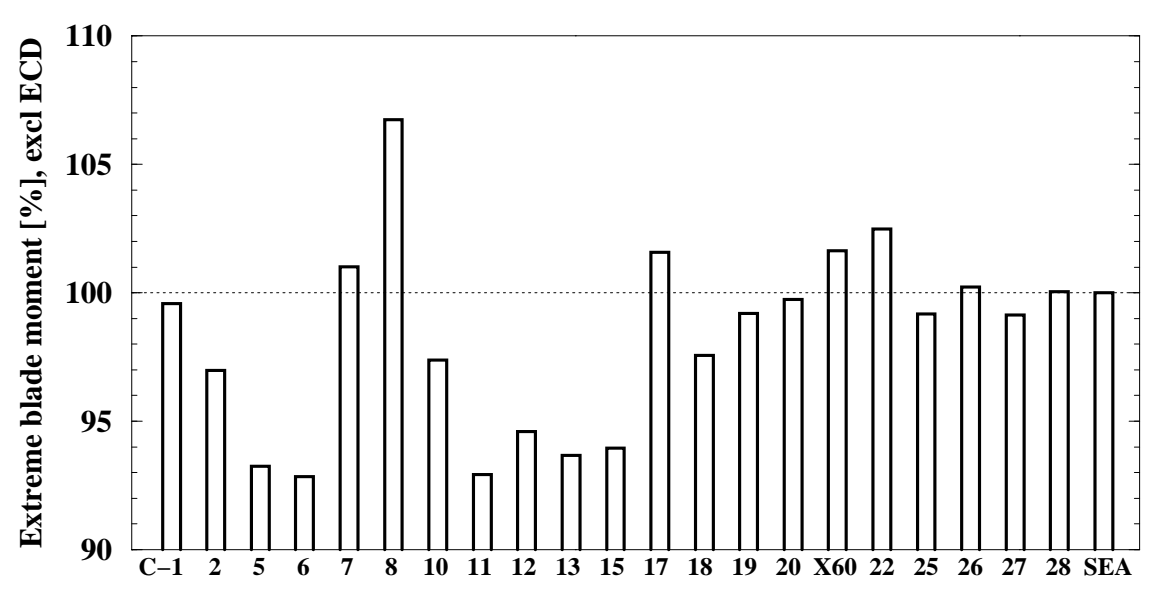


Figure 4.6 Extreme blade root moments for the configurations, excluding ECD

occur in load case file 131. Investigation to the dynamic response in this file 131 (ECD: "Extreme

Coherent gust and Direction change") shows that for this load case all configurations are initially just below nominal power while configuration *C-07* (10% wider chord) operates just at the nominal power. The coherent gust gives a rise in rotor-speed which causes the controller to pitch the blades to vane. Finally the wind direction change gives a reduction in power and thus a reduction in rotor speed which causes the controller to pitch the blades back. For operation with misalignment, the extreme blade moments are proportional to rotor speed. For configuration *C-07* this second pitch action is less strong while the drop in rotor speed is stronger than for the other configurations.

For the baseline blade LMH46-5-X00 and for the 110% wide blade LMH46-5-X02 (configurations *C-00* and *C-07*) the response for DLC 1.3 is calculated for a number of wind speed values around nominal. The resulting extreme blade root moments are made dimensionless by the extreme moment for the wind speed of 11.5m/s.

it for the wind	speed of 11.5m/c	,.	
Ambient	C-07, extreme	C-00, extreme	C-00, reduced
wind speed	root moment	root moment	speed limit
11.0m/s	-0.16%	+8.17%	+7.88%
11.1m/s	-9.00%	+9.93%	+9.61%
11.2m/s	-18.01%	+11.08%	+1.20%
11.3m/s	-7.77%	+12.92%	+12.48%
11.4m/s	-7.11%	+12.87%	+10.48%
11.5m/s	-8.98%	100%	-6.61%
11.6m/s	-11.59%	+4.19%	-0.26%
11.7m/s	-6.72%	-8.68%	-11.73%
11.8m/s	-14.91%	-14.15%	-18.71%
11.9m/s	-15.96%	-12.11%	-17.70%
12.0m/s	-15.37%	-10.51%	-13.28%
12.5m/s	-21.77%	-18.94%	-20.31%
13.0m/s	-28.59%	-26.52%	-24.54%

From this table it follows that for configuration *C-00* the extreme moment is found for 11.3m/s while for the 110% wide blade X02 the extreme moment occurs for 11.0m/s. Although the trend is not smooth, the extreme moment shows a serious reduction if the wind speed increases above nominal. The wind speed for the extreme moment shows a dependency with the value of the nominal wind speed which is 11.6m/s and 11.4m/s for configuration *C-00* and *C-07* respectively.

The calculated dynamic response for this load case at a wind speed above nominal shows that the rotor speed exceeds the limit at which the controller pitches the blades fast to vane. As a result the pitch angle during the following seconds is somewhat larger which results in smaller extreme flap bending moments. It can be concluded that lowering the 'rotor speed limit' ('Fuzzy limit') for fast control actions may reduce the extreme blade moments. To investigate this effect, the dynamic response is also calculated for a 0.2rpm lower 'rotor speed limit', of which the extreme blade root moments are written in the last column of the table. The extreme moments in the last column are made dimensionless with the extreme moments in load case file 131 (11.5m/s) for the baseline configuration *C-00* with the LMH46-5-X00 blades. From the last column in the table it follows that the fast pitch actions take place at smaller wind speeds compared to the "baseline" controller settings. The result is a smaller extreme blade root moment.

Finally the dynamic response on the 'Extreme Coherent gust and Direction change', IEC gust 'ECD', for configuration *C-00* is calculated in which the maximum pitch rate to working position is varied. The results of these calculations give the following extreme root moments.

Pitch rate to	Extreme
working pos.	root moment
-5.5deg/s	+4.98%
-5.0deg/s	100%
-4.5deg/s	-6.62%
-4.0deg/s	-10.80%
-3.5deg/s	-10.80%

From this continuous relation up to -4.0deg/s and from the previous table it is concluded that modifications of the control algorithm can reduce the extreme blade loads. Using a reduced pitch rate to vane as in the last table is a modification that gives conservative loads in "gusty" winds, although it may imply some loss of 'control efficiency'.

One should be careful with controller modifications on basis of a single load case since one may be tuning the control algorithm for only the shape of the idealised IEC gust.

4.2.6 Extreme flatwise blade moments

Assuming that the control algorithm is adjusted in order to avoid extreme moments for "gusty" wind variations as in DLC 1.3, the extreme flatwise moments in the blade are found as:

	Extreme overall flatwise moments						
Configuration R=1.5m file R=20m file R=35m							
C-00: LMH46-5-X00 "baseline"	100%	161	100%	161	100%	162	
C-01: X00, Former baseline, n.o.t.	-2.40%	161	-11.85%	115	-5.95%	123	
C-02: X03: DU 96-W-180 airfoil	-3.24%	161	-15.38%	161	-17.66%	114	
C-05: X01: 90% slender chord	-8.91%	116	-18.32%	162	-7.61%	157	
C-06: X01: 90% chord, 81% stiffn.	-10.11%	161	-19.90%	162	-12.16%	162	
C-07: X02: 110% wide chord	+1.14%	115	-2.03%	123	+19.73%	123	
C-08: X02: 110% chord, 121% stiffn.	+7.22%	821	+0.66%	156	+12.65%	162	
C-10: X00, 86.6% speed, n.o.t.	-4.20%	722	-18.48%	191	-7.46%	162	
C-11: X00, 86.6% sub-optimal speed	-7.31%	822	-20.54%	112	-4.00%	123	
C-12: X00, 90.3% speed, n.o.t.	-7.08%	191	-18.69%	156	-3.71%	123	
C-13: X00, 90.3% sub-optimal speed	-6.85%	811	-19.03%	811	-10.09%	156	
C-15: X00, 93.3% sub-optimal speed	-8.07%	191	-18.14%	161	-1.36%	162	
C-17: Tip speed 79m/s, 95% chord	+0.17%	161	-11.21%	162	-0.01%	162	
C-18: Tip speed 79m/s, 90% chord	-6.88%	172	-17.65%	172	-5.16%	162	
C-19: Tapered modification 1 of X00	-0.55%	161	-10.05%	115	-3.38%	157	
C-20: Tapered modification 2 of X00	-0.03%	161	-12.80%	161	-4.48%	162	
<i>C-21</i> : LMH46-5-X60 , Re= $7 \cdot 10^6$, <i>n.o.t.</i>	+1.03%	161	-6.75%	115	-11.45%	162	
C-22: LMH46-5-X00, Re= $7 \cdot 10^6$, n.o.t.	+2.49%	161	-5.95%	161	-6.03%	162	
C-25: X00, no pre-bending	-3.23%	161	-9.55%	157	+0.66%	162	
C-26: X00, with model for pre-bend	+0.23%	161	-7.03%	161	-5.64%	162	
C-27: X00, 4% tower damping	-0.82%	161	-11.05%	157	+0.06%	162	
C-28: X00, modelling shaft torsion	+0.02%	161	-9.12%	115	-0.07%	162	
C-29: X00, low turbulence: "SEA"	+0.00%	161	+3.87%	132	+69.75%	630	

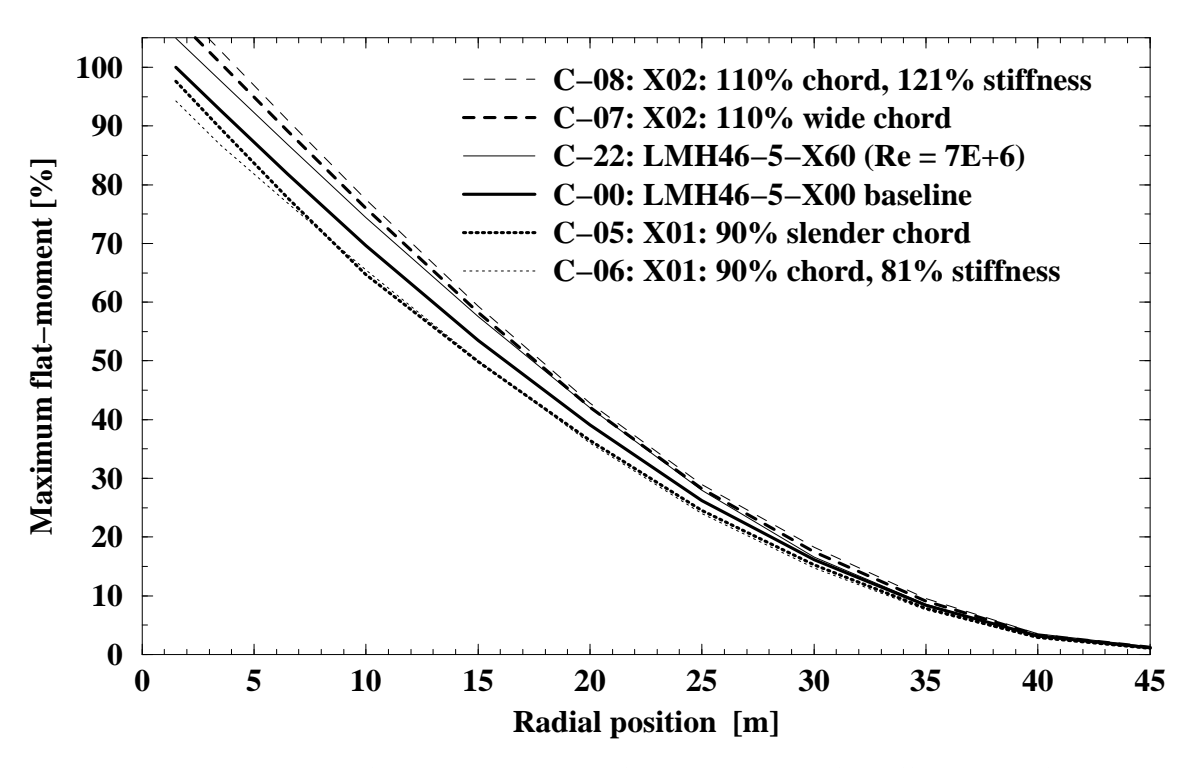


Figure 4.7 Distribution of production-extreme flatwise moments for different plan-forms

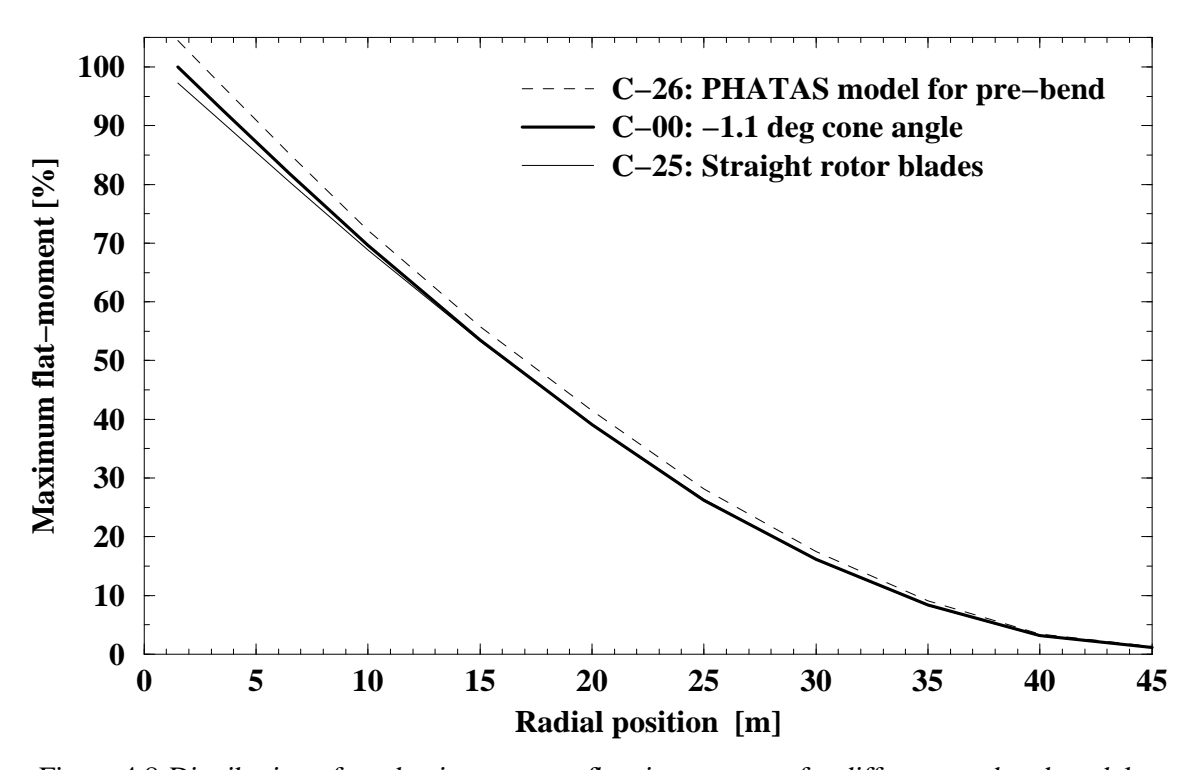


Figure 4.8 Distribution of production-extreme flatwise moments for different pre-bend models

4.2.7 Minimum tower clearance

The tower clearance is the minimum distance of the blade tip to the outer radius of the tower.

This is determined for all three rotor blades.

Power Load | Overall Load

	Power	Load	Overall	Load
Configuration	production	case	clearance	case
C-00: LMH46-5-X00 "baseline"	reference	113	<—	
C-02: X03: DU 96-W-180 airfoil	+0.16m	113	<	
C-05: X01: 90% slender chord	+0.36m	115	<	
C-06: X01: 90% chord, 81% stiffn.	-0.80m	113	<	
C-07: X02: 110% wide chord	-0.01m	111	<—	
C-08: X02: 110% chord, 121% stiffn.	+0.65m	113	<	
C-10: X00, 86.6% speed, n.o.t.	+0.41m	113	-0.65m	132
C-11: X00, 86.6% sub-optimal speed	+0.13m	115	-0.55m	132
C-12: X00, 90.3% speed, n.o.t.	-0.08m	115	-0.21m	132
C-13: X00, 90.3% sub-optimal speed	+0.22m	113	-0.23m	132
C-15: X00, 93.3% sub-optimal speed	+0.03m	115	-0.35m	132
C-17: Tip speed 79m/s, 95% chord	+0.12m	113	-0.02m	132
C-18: Tip speed 79m/s, 90% chord	+0.36m	111	<	
C-19: Tapered modification 1 of X00	+0.18m	113	<—	
C-20: Tapered modification 2 of X00	+0.04m	113	<	
C-21: LMH46-5-X60 , Re= $7 \cdot 10^6$, n.o.t.	+1.09m	113	+1.02m	132
C-22: LMH46-5-X00, Re= $7 \cdot 10^6$, n.o.t.	+0.98m	113	+0.89m	132
C-25: X00, no pre-bending	-0.66m	113	<	
C-26: X00, with model for pre-bend	+0.73m	113	<	
C-27: X00, 4% tower damping	-0.05m	113	<	
C-28: X00, modelling shaft torsion	+0.12m	111	<	
C-29: X00, low turbulence: "SEA"	+0.73m	112	+0.48m	152
	. 11		4.4	

This table shows that load cases with a positive misalignment give the smallest tower clearances, while the previous tables show that load cases with a negative misalignment give the largest rotor blade loads.

Load case DLC 1.7 has also been calculated with a negative vertical shear variation (file 174) because this may give a small tower clearance. This tower clearance however has shown to be not the most critical.

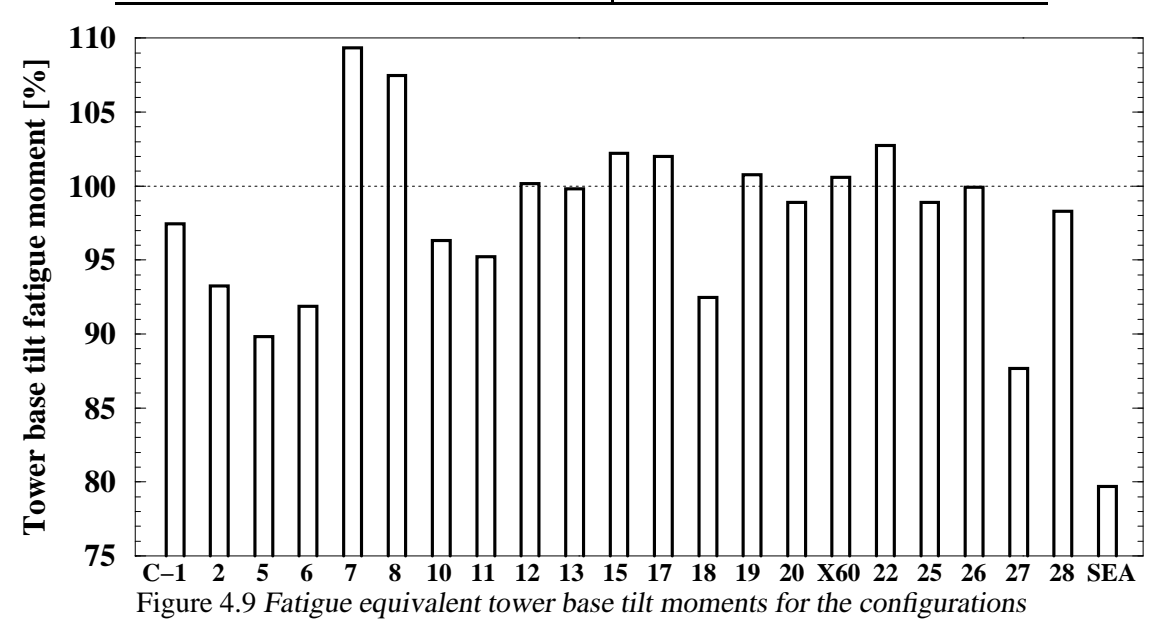
4.3 Fatigue Loads

From the calculated load cases for production and for stand by above cut-out wind speed, the 1Hz fatigue equivalent load cycles are calculated for a Weibull average of 10m/s.

4.3.1 Tower fore-aft loads

The fatigue equivalent cycles for the tower are calculated for a $\log S - \log N$ damage function with a slope parameter m = 1/3.

	Moment	Moment	Axial force
Configuration	at base	at top	at top
C-00: LMH46-5-X00 "baseline"	100%	100%	100%
C-01: X00, Former baseline, n.o.t.	-2.55%	+0.45%	-1.60%
C-02: X03: DU 96-W-180 airfoil	-6.74%	-1.00%	-5.88%
C-05: X01: 90% slender chord	-10.18%	-7.01%	-9.46%
C-06: X01: 90% chord, 81% stiffn.	-8.14%	-10.61%	-6.85%
C-07: X02: 110% wide chord	+9.36%	+6.76%	+9.01%
C-08: X02: 110% chord, 121% stiffn.	+7.49%	+12.31%	+7.04%
C-10: X00, 86.6% speed, n.o.t.	-3.67%	-11.32%	-7.62%
C-11: X00, 86.6% sub-optimal speed	-4.79%	-9.84%	-8.23%
C-12: X00, 90.3% speed, n.o.t.	+0.16%	-6.98%	-3.05%
C-13: X00, 90.3% sub-optimal speed	-0.19%	-8.63%	-3.56%
C-15: X00, 93.3% sub-optimal speed	+2.22%	-6.52%	-0.78%
C-17: Tip speed 79m/s, 95% chord	+1.99%	+1.25%	+3.02%
C-18: Tip speed 79m/s, 90% chord	-7.52%	-1.73%	-5.21%
C-19: Tapered modification 1 of X00	+0.78%	-0.42%	+0.64%
C-20: Tapered modification 2 of X00	-1.09%	-1.03%	-1.23%
C-21: LMH46-5-X60 , Re= $7 \cdot 10^6$, n.o.t.	+0.59%	-1.21%	-0.29%
C-22: LMH46-5-X00, Re= $7 \cdot 10^6$, n.o.t.	+2.75%	+0.69%	+2.25%
C-25: X00, no pre-bending	-1.12%	-0.77%	-1.05%
C-26: X00, with model for pre-bend	-0.08%	-0.05%	-0.22%
C-27: X00, 4% tower damping	-12.34%	-3.33%	-13.80%
C-28: X00, modelling shaft torsion	-1.71%	-0.32%	-1.16%
C-29: X00, low turbulence: "SEA"	-20.32%	-28.00%	-21.78%



4.3.2 Tower side loads

	Moment	Moment	Side force
Configuration	at base	at top	at top
C-00: LMH46-5-X00 "baseline"	100%	100%	100%
C-01: X00, Former baseline, n.o.t.	-0.57%	+0.38%	+2.37%
C-02: X03: DU 96-W-180 airfoil	-3.45%	-3.25%	-2.21%
C-05: X01: 90% slender chord	-8.14%	-4.48%	-4.16%
C-06: X01: 90% chord, 81% stiffn.	-10.04%	-13.41%	-11.85%
C-07: X02: 110% wide chord	+6.07%	+3.57%	+6.17%
C-08: X02: 110% chord, 121% stiffn.	+25.29%	+34.38%	+42.92%
C-10: X00, 86.6% speed, n.o.t.	-5.42%	-2.59%	-10.79%
C-11: X00, 86.6% sub-optimal speed	-2.00%	-6.02%	-10.32%
C-12: X00, 90.3% speed, n.o.t.	-3.35%	-1.22%	-7.49%
C-13: X00, 90.3% sub-optimal speed	-5.21%	-6.29%	-11.34%
C-15: X00, 93.3% sub-optimal speed	-1.74%	+1.48%	-5.23%
C-17: Tip speed 79m/s, 95% chord	-3.12%	-5.47%	+0.96%
C-18: Tip speed 79m/s, 90% chord	-5.90%	-6.83%	-0.27%
C-19: Tapered modification 1 of X00	-3.20%	-1.82%	-1.62%
C-20: Tapered modification 2 of X00	+0.73%	-2.69%	-0.25%
C-21: LMH46-5-X60 , Re= $7 \cdot 10^6$, n.o.t.	-2.18%	-4.99%	-2.60%
C-22: LMH46-5-X00, Re= $7 \cdot 10^6$, n.o.t.	+0.62%	-3.82%	-0.71%
C-25: X00, no pre-bending	-0.41%	+0.01%	+1.42%
C-26: X00, with model for pre-bend	-3.53%	-3.78%	-2.72%
C-27: X00, 4% tower damping	-51.46%	-31.96%	-49.85%
C-28: X00, modelling shaft torsion	+2.71%	+53.12%	+9.33%
C-29: X00, low turbulence: "SEA"	-19.49%	-24.48%	-25.04%

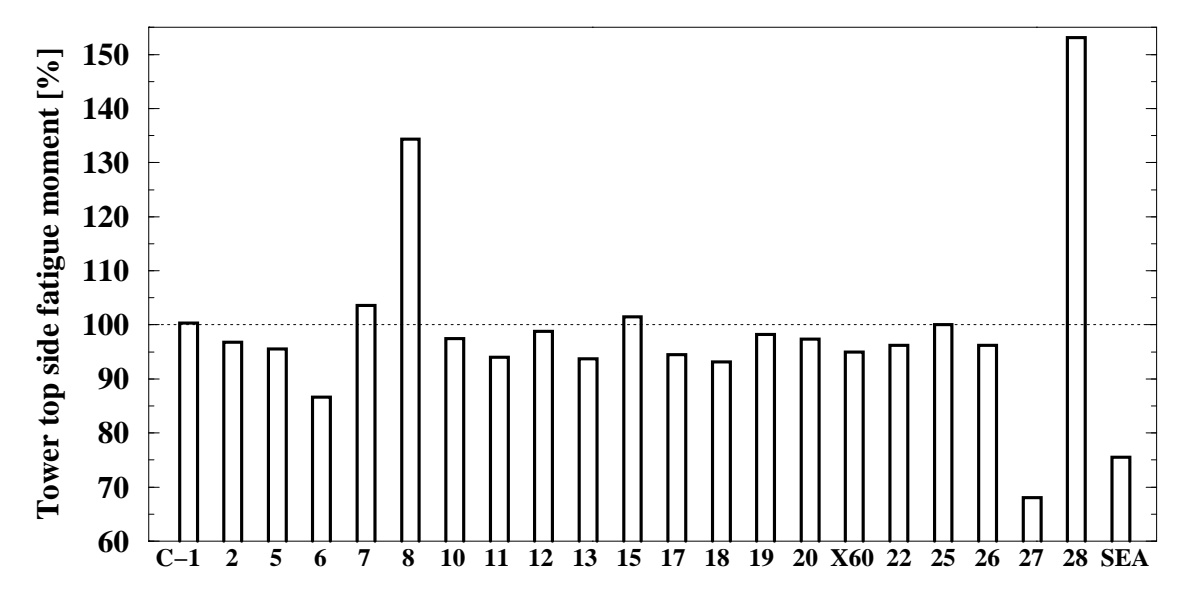


Figure 4.10 Fatigue equivalent tower top side moments for the configurations

4.3.3 Non-rotating shaft loads

The non-rotating shaft loads 1.8m behind the rotor centre are calculated with a $\log S - \log N$ damage function with a slope parameter m = 1/3.

	Tilt	Axial	Side	Vertical
Configuration	moment	force	force	force
C-00: LMH46-5-X00 "baseline"	100%	100%	100%	100%
C-01: X00, Former baseline, n.o.t.	+0.45%	-0.54%	+1.58%	+2.12%
C-02: X03: DU 96-W-180 airfoil	-1.05%	-3.33%	-0.40%	+0.40%
C-05: X01: 90% slender chord	-7.12%	-9.28%	-4.60%	-3.16%
C-06: X01: 90% chord, 81% stiffn.	-11.07%	-9.62%	-9.45%	-7.06%
C-07: X02: 110% wide chord	+6.51%	+9.60%	+4.98%	+4.28%
C-08: X02: 110% chord, 121% stiffn.	+11.18%	+9.21%	+8.58%	+20.03%
C-10: X00, 86.6% speed, n.o.t.	-12.25%	-7.55%	-13.11%	-12.69%
C-11: X00, 86.6% sub-optimal speed	-10.52%	-7.25%	-13.54%	-14.97%
C-12: X00, 90.3% speed, n.o.t.	-8.13%	-3.66%	-7.76%	-6.55%
C-13: X00, 90.3% sub-optimal speed	-9.57%	-4.01%	-9.90%	-9.48%
C-15: X00, 93.3% sub-optimal speed	-7.45%	-0.95%	-5.72%	-4.66%
C-17: Tip speed 79m/s, 95% chord	+1.57%	+2.38%	+2.60%	+0.45%
C-18: Tip speed 79m/s, 90% chord	-1.35%	-5.57%	+0.09%	-1.43%
C-19: Tapered modification 1 of X00	-0.67%	+0.92%	-0.65%	+0.57%
C-20: Tapered modification 2 of X00	-1.10%	-0.53%	-1.19%	-0.74%
C-21: LMH46-5-X60 , Re= $7 \cdot 10^6$, n.o.t.	-1.52%	+1.01%	-1.74%	-2.98%
C-22: LMH46-5-X00, Re= $7 \cdot 10^6$, n.o.t.	+0.45%	+2.56%	-0.10%	-1.03%
C-25: X00, no pre-bending	-0.55%	-0.65%	+0.28%	+0.27%
C-26: X00, with model for pre-bend	-0.12%	+0.29%	-0.39%	-1.70%
C-27: X00, 4% tower damping	-1.65%	-3.28%	-6.14%	-8.67%
C-28: X00, modelling shaft torsion	-0.33%	-1.14%	-0.63%	-0.93%
C-29: X00, low turbulence: "SEA"	-28.03%	-23.98%	-28.88%	-30.05%

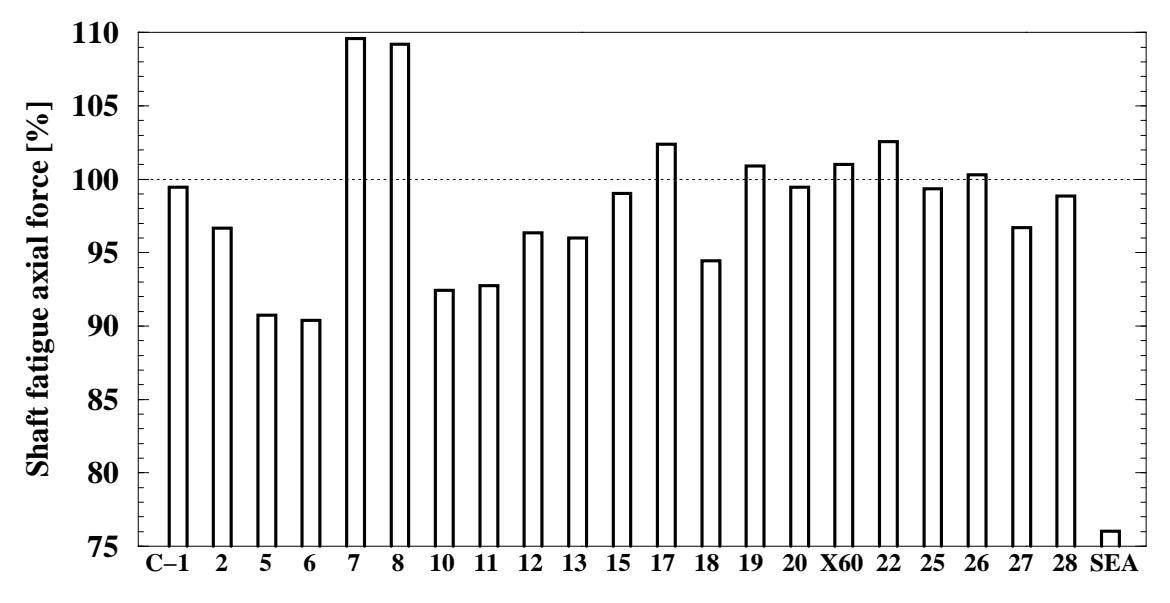


Figure 4.11 Shaft fatigue axial forces for the configurations

4.3.4 Rotating shaft moments

The rotating shaft moments 1.8m behind the rotor centre are.

	Shaft	Moment	Moment
Configuration	Torque	1	2
C-00: LMH46-5-X00 "baseline"	100%	100%	100%
C-01: X00, Former baseline, n.o.t.	+1.08%	+0.53%	+0.39%
C-02: X03: DU 96-W-180 airfoil	-1.23%	-0.67%	-0.47%
C-05: X01: 90% slender chord	-3.13%	-4.21%	-4.16%
C-06: X01: 90% chord, 81% stiffn.	-7.74%	-6.32%	-6.67%
C-07: X02: 110% wide chord	+5.36%	+4.54%	+4.70%
C-08: X02: 110% chord, 121% stiffn.	+26.77%	+7.05%	+6.95%
C-10: X00, 86.6% speed, n.o.t.	+11.58%	-8.24%	-8.49%
C-11: X00, 86.6% sub-optimal speed	+7.15%	-7.45%	-7.59%
C-12: X00, 90.3% speed, n.o.t.	+8.81%	-6.04%	-5.43%
C-13: X00, 90.3% sub-optimal speed	+2.19%	-6.70%	-6.54%
C-15: X00, 93.3% sub-optimal speed	+7.76%	-4.99%	-5.52%
C-17: Tip speed 79m/s, 95% chord	-5.53%	+1.82%	+1.71%
C-18: Tip speed 79m/s, 90% chord	-9.61%	-0.25%	-0.29%
C-19: Tapered modification 1 of X00	+0.56%	-0.44%	-0.30%
C-20: Tapered modification 2 of X00	-0.04%	-0.71%	-0.45%
C-21: LMH46-5-X60 , Re= $7 \cdot 10^6$, n.o.t.	-3.70%	-2.75%	-2.71%
C-22: LMH46-5-X00, Re= $7 \cdot 10^6$, n.o.t.	-2.52%	-1.34%	-1.28%
C-25: X00, no pre-bending	+1.09%	-2.69%	-2.70%
C-26: X00, with model for pre-bend	-2.20%	-2.11%	-1.77%
C-27: X00, 4% tower damping	-21.63%	-0.73%	-0.47%
C-28: X00, modelling shaft torsion	+72.42%	-0.21%	+0.05%
C-29: X00, low turbulence: "SEA"	-19.80%	-22.81%	-23.08%

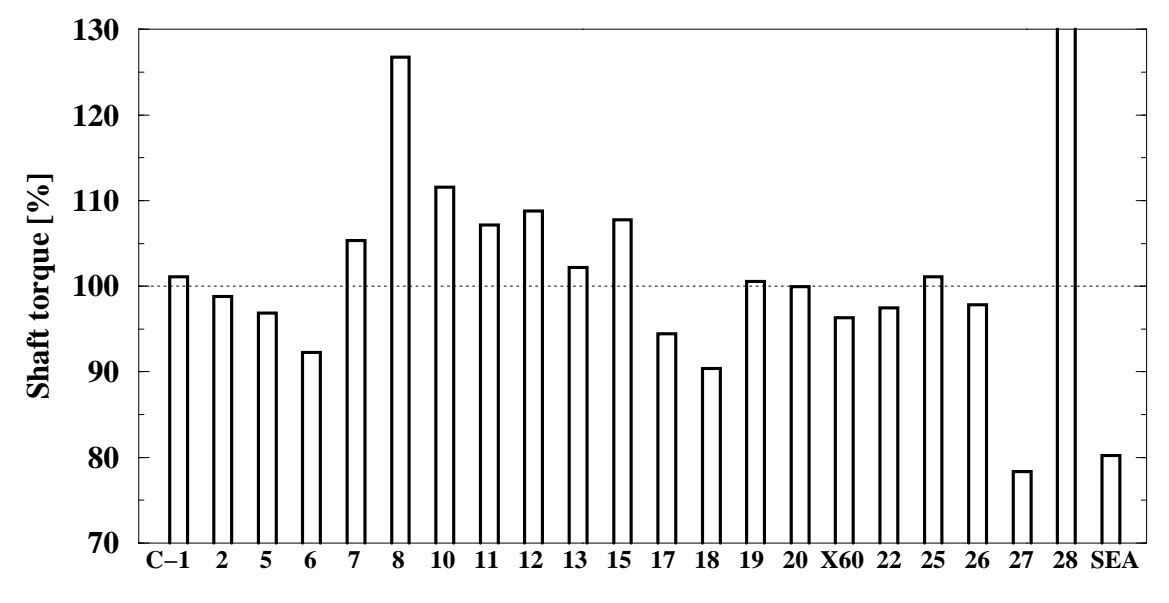


Figure 4.12 Shaft torque fatigue moments for the configurations

4.3.5 Blade loads

The fatigue equivalent flatwise moments are calculated with a $\log S - \log N$ damage function with a slope parameter m = 1/10. In order to reduce the scatter in the fatigue equivalent cycles, the load time series from all three blades are used.

Configuration	R = 1.5m	R = 20m	R = 35m
C-00: LMH46-5-X00 "baseline"	100%	100%	100%
C-01: X00, Former baseline, n.o.t.	+1.21%	+2.41%	+5.03%
C-02: X03: DU 96-W-180 airfoil	-6.32%	-8.93%	-8.75%
C-05: X01: 90% slender chord	-6.86%	-6.51%	-4.45%
C-06: X01: 90% chord, 81% stiffn.	-8.77%	-9.91%	-8.04%
C-07: X02: 110% wide chord	+8.99%	+9.56%	+11.68%
C-08: X02: 110% chord, 121% stiffn.	+9.27%	+11.84%	+14.83%
C-10: X00, 86.6% speed, n.o.t.	-6.36%	-5.65%	-1.87%
C-11: X00, 86.6% sub-optimal speed	-4.26%	-4.94%	-2.00%
C-12: X00, 90.3% speed, n.o.t.	-2.32%	-1.76%	+1.53%
C-13: X00, 90.3% sub-optimal speed	-4.98%	-4.09%	-1.22%
C-15: X00, 93.3% sub-optimal speed	-4.07%	-2.89%	+0.67%
C-17: Tip speed 79m/s, 95% chord	+0.20%	-0.33%	+1.79%
C-18: Tip speed 79m/s, 90% chord	-5.27%	-6.13%	-4.50%
C-19: Tapered modification 1 of X00	-0.76%	-1.97%	-0.81%
C-20: Tapered modification 2 of X00	-1.02%	-2.04%	-1.68%
C-21: LMH46-5-X60 , Re=7·10 ⁶ , n.o.t.	-1.08%	-3.02%	-2.14%
C-22: LMH46-5-X00, Re= $7 \cdot 10^6$, n.o.t.	+0.99%	-0.79%	+1.84%
C-25: X00, no pre-bending	-0.73%	-0.72%	+1.56%
C-26: X00, with model for pre-bend	-0.15%	-0.80%	+1.04%
C-27: X00, 4% tower damping	-1.04%	-0.09%	+2.06%
C-28: X00, modelling shaft torsion	-0.93%	-1.25%	+0.71%
C-29: X00, low turbulence: "SEA"	-11.56%	-1.71%	+31.83%

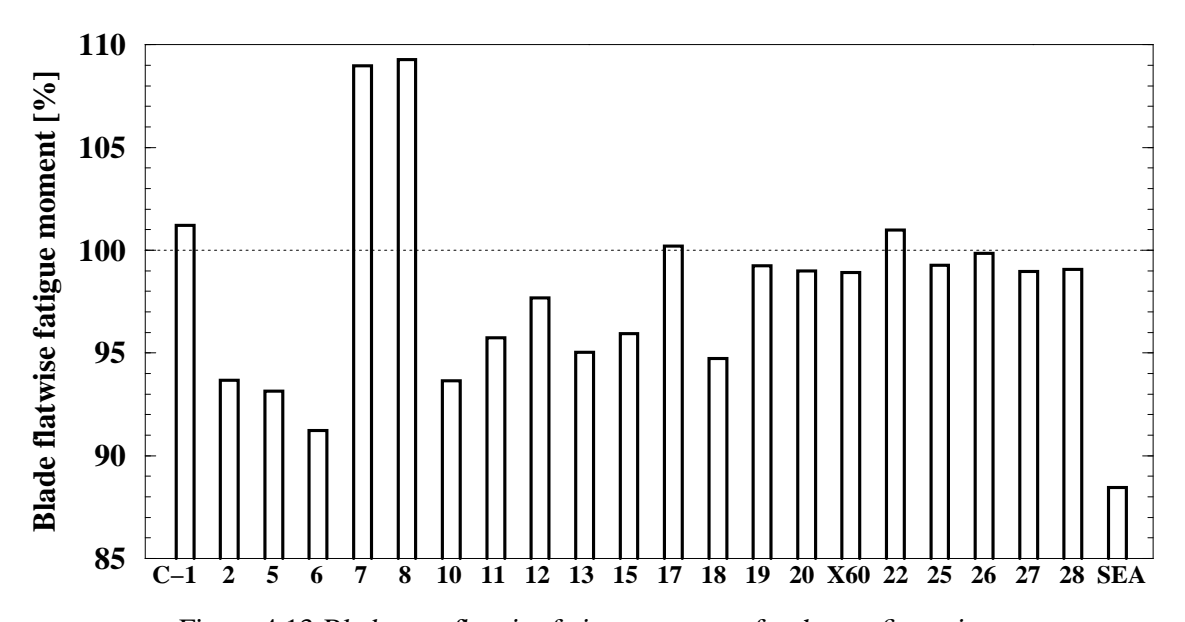


Figure 4.13 Blade root flatwise fatigue moments for the configurations

The fatigue equivalent edgewise moments are calculated from the load time series of all three blades using a slope parameter m = 1/10.

Configuration	R = 1.5m	R = 20m	R = 35m
C-00: LMH46-5-X00 "baseline"	100%	100%	100%
C-01: X00, Former baseline, n.o.t.	+1.22%	+1.92%	+1.65%
C-02: X03: DU 96-W-180 airfoil	+0.48%	+3.02%	+17.68%
C-05: X01: 90% slender chord	-1.24%	-0.99%	-2.96%
C-06: X01: 90% chord, 81% stiffn.	-1.36%	-0.24%	-0.02%
C-07: X02: 110% wide chord	+0.75%	+1.62%	+3.11%
C-08: X02: 110% chord, 121% stiffn.	+0.98%	+1.90%	+2.22%
C-10: X00, 86.6% speed, n.o.t.	-4.22%	-4.28%	+32.56%
C-11: X00, 86.6% sub-optimal speed	-8.22%	-9.03%	-10.18%
C-12: X00, 90.3% speed, n.o.t.	-5.56%	-6.64%	-8.03%
C-13: X00, 90.3% sub-optimal speed	-6.65%	-7.73%	-9.20%
C-15: X00, 93.3% sub-optimal speed	-4.73%	-6.17%	-8.08%
C-17: Tip speed 79m/s, 95% chord	+3.56%	+7.30%	+7.53%
C-18: Tip speed 79m/s, 90% chord	+2.58%	+6.09%	+5.66%
C-19: Tapered modification 1 of X00	+5.91%	+16.06%	+74.03%
C-20: Tapered modification 2 of X00	-0.22%	+0.61%	-0.39%
C-21: LMH46-5-X60 , Re= $7 \cdot 10^6$, n.o.t.	-0.04%	+1.04%	+2.22%
C-22: LMH46-5-X00, Re= $7 \cdot 10^6$, n.o.t.	+0.46%	+1.64%	+1.07%
C-25: X00, no pre-bending	-0.73%	-0.42%	-0.92%
C-26: X00, with model for pre-bend	-0.77%	-0.32%	-0.65%
C-27: X00, 4% tower damping	-1.78%	-2.51%	-3.94%
C-28: X00, modelling shaft torsion	-0.18%	+0.23%	+1.78%
C-29: X00, low turbulence: "SEA"	-8.68%	-9.59%	+25.88%

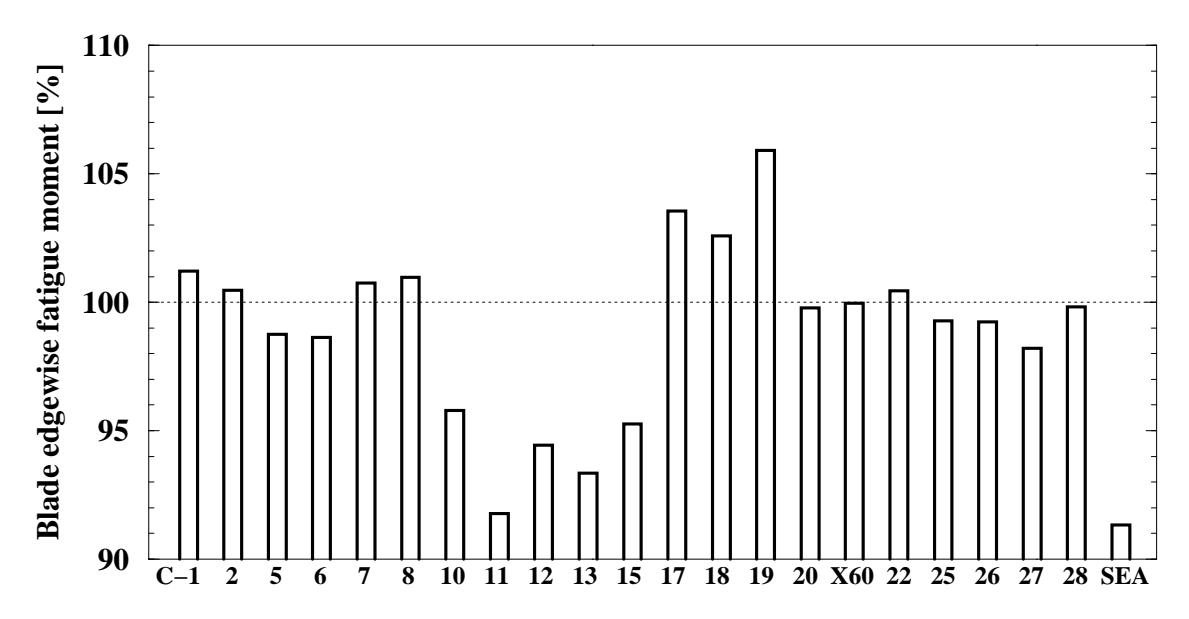


Figure 4.14 Blade root edgewise fatigue moments for the configurations

The large fatigue equivalent edgewise moments at radius 35m for the configurations C-02 and C-19 have shown to be caused by edgewise vibrations in blade 3, which in the calculation has a pitch error of -0.5deg. With this pitch error the angle of attack is slightly higher. The loads for blade 3 are the worst for the production load cases at 17, 19, 21 and 23m/s for which the misalignment is positive (downwind blade is advancing the wind).

Investigations will be performed to the reason of the increased loads.

5. ESTIMATED COST OF ENERGY

The cost-of-energy estimates reported in this chapter are obtained with the annual yield and with the extreme and fatigue loads from the calculated dynamic load sets. The relations between cost and loads are based on an assumed cost-breakdown and load-dependency, since detailed machine data were not yet known.

5.1 Cost Estimation as Function of Design Loads

For the estimated cost of energy the load depending cost-contributions are defined.

The cost breakdown of the turbine is obtained through Don den Hoed.

The load dependencies have been obtained through Frank Goezinne.

The cost breakdown for offshore is calculated assuming that the turbine investment amounts to one third of the total investment and assuming a margin of 20% and some minor overhead costs.

	Percentage	Percentage	Design driving	Load
	wind turbine	offshore farm	load component	component
Component	compon. cost	sales price		cost fraction
Rotor	24.00%	6.28%	M_(blade root), Extr.	25%
			M_(edge, root), Fat.	25%
Main shaft	4.02%	1.05%	Rotor mass (not used)	75%
Yaw system	5.00%	1.31%		
Gear system	16.00%	4.19%	Torque level	75%
			Rotor thrust, Fat.	10%
Gener. & invert.	10.00%	2.62%		
Brake system	0.77%	0.20%		
Main frame	3.15%	0.82%	M_(tilt, rotor), Fat.	35%
			Shaft torque, Fat.	25%
			Rotor thrust, Fat.	25%
Cover & spinner	1.67%	0.44%		
Nacelle assembly	0.39%	0.10%		
Cooling system	0.90%	0.23%		
Control system	5.00%	1.31%		
HV installation	3.50%	0.92%		
Tower	25.00%	6.55%	M_(tilt, base), Extr.	40%
			M_(tilt, top), Extr.	30%
Other	0.60%	0.16%		
Total	100.00%	26.18%		41 4 1: 1

In the calculation of the price performance ratio the relative component costs are the costs divided by those for the baseline configuration C-00. Similarly the relative yield is the yield divided by the yield for the baseline. Finally the cost of energy is the sum of component costs divided by the yield, which is finally expressed with respect to the cost of energy for the baseline.

The extreme tower moments for configuration *C-15* (93.3% sub-optimal speed) are the extreme moments without load case 611, assuming that the free-yawing response will finally be designed on small idling loads.

5.2 Cost of Energy for each Configuration

	Estimate	ed turbine	e costs:	Energy	Cost of Energy:
Configuration	Fatigue	Extreme	Total	capture	Turbine Farm
C-00: LMH46-5-X00 "baseline"	100%	100%	100%	100%	100% 100%
C-01: X00, Former baseline, n.o.t.	+0.11%	-1.23%	-1.12%	-0.29%	-0.84% -0.01%
C-02: X03: DU 96-W-180 airfoil	-0.15%	-1.59%	-1.73%	-0.37%	-1.36% -0.08%
C-05: X01: 90% slender chord	-0.93%	-0.95%	-1.87%	-2.09%	+0.23% +1.64%
C-06: X01: 90% chord, 81% stiffn.	-1.29%	-0.95%	-2.24%	-2.08%	-0.17% +1.52%
C-07: X02: 110% wide chord	+0.90%	-0.16%	+0.73%	+0.79%	-0.05% -0.59%
C-08: X02: 110% chord, 121% stiffn.	+1.54%	+0.90%	+2.43%	+0.73%	+1.69% -0.09%
C-10: X00, 86.6% speed, n.o.t.	+0.53%	-1.48%	-0.95%	-7.16%	+6.69% +7.45%
C-11: X00, 86.6% sub-optimal speed	+0.39%	-1.37%	-0.97%	-5.96%	+5.31% +6.07%
C-12: X00, 90.3% speed, n.o.t.	+0.32%	-1.38%	-1.06%	-3.98%	+3.05% +3.86%
C-13: X00, 90.3% sub-optimal speed	+0.06%	-1.27%	-1.22%	-4.05%	+2.95% +3.89%
C-15: X00, 93.3% sub-optimal speed	+0.05%	-0.84%	-0.79%	-3.11%	+2.39% +2.99%
C-17: Tip speed 79m/s, 95% chord	-0.27%	+0.75%	+0.48%	+0.38%	+0.10% -0.26%
C-18: Tip speed 79m/s, 90% chord	-0.81%	+0.29%	-0.52%	-0.71%	+0.19% +0.58%
C-19: Tapered modification 1 of X00	+0.34%	-0.03%	+0.31%	-0.12%	+0.43% +0.20%
C-20: Tapered modification 2 of X00	-0.12%	+0.04%	-0.08%	-0.14%	+0.06% +0.12%
C-21: LMH46-5-X60 , Re= $7 \cdot 10^6$, n.o.t.	-0.12%	+0.35%	+0.24%	-0.23%	+0.47% +0.30%
C-22: LMH46-5-X00, Re= $7 \cdot 10^6$, n.o.t.	+0.13%	+0.31%	+0.44%	+0.57%	-0.14% -0.46%
C-25: X00, no pre-bending	-0.11%	-0.04%	-0.15%	+0.03%	-0.18% -0.07%
C-26: X00, with model for pre-bend	-0.06%	001%	-0.06%	-0.05%	-0.01% +0.04%
C-27: X00, 4% tower damping	-0.62%	-0.98%	-1.61%	-0.00%	-1.61% -0.42%
C-28: X00, modelling shaft torsion	+0.50%	+.006%	+0.51%	-0.08%	+0.60% +0.22%
C-29: X00, low turbulence: "SEA"	-3.66%	+0.0%	-3.66%	-1.58%	-2.11% +0.64%

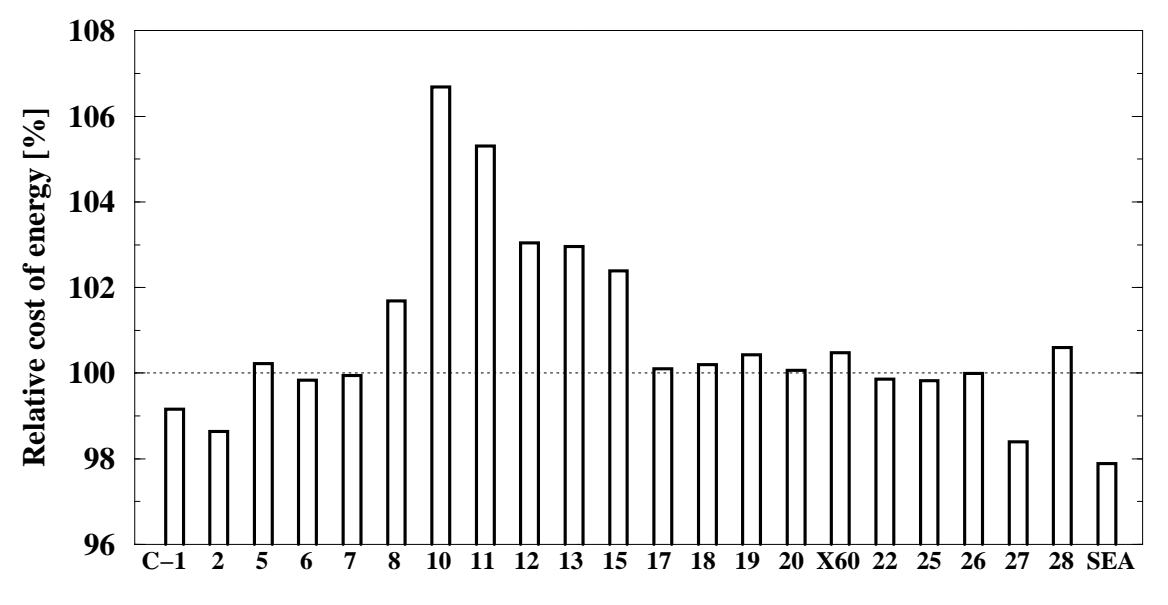


Figure 5.1 Estimated turbine cost of energy

The relative cost of energy for a turbine and for a wind farm are plotted in figure 5.1 and figure 5.2. Comparison of figure 5.1 and 5.2 shows that the smaller (26.28%) fraction of the turbine loads on the farm cost gives a slightly different ranking for the configurations.

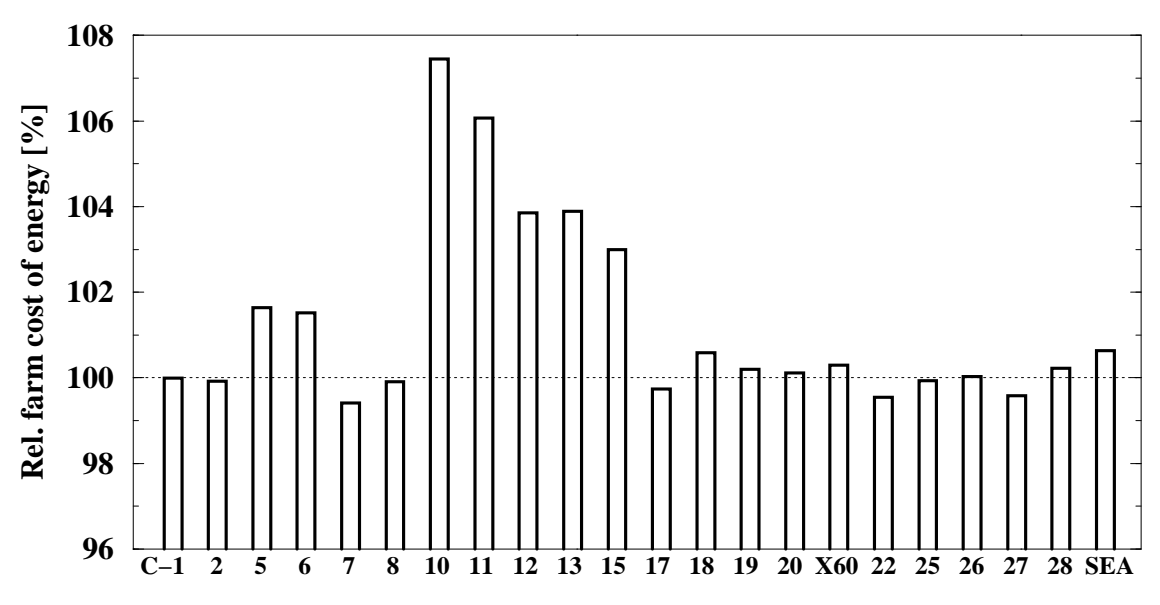


Figure 5.2 Estimated wind farm cost of energy

5.3 Cost of Energy versus Blade Chord

For the configurations with more slender or more wide blade, figure 5.3 shows the cost of energy as function of blade chord, all relative to the baseline configuration *C-00*.

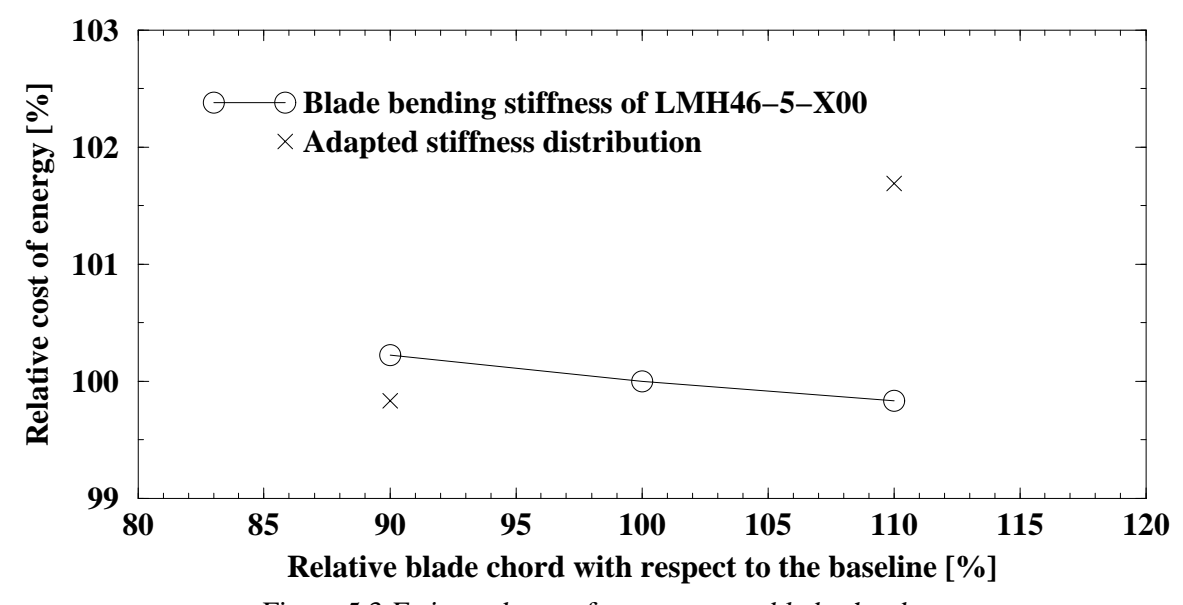


Figure 5.3 Estimated cost of energy versus blade chord

As can be seen from this figure, the three points show a small decreasing cost of energy for a wider chord. The adapted stiffness values show however that more slender (more flexible) blades give a reduction in cost of energy. For the influence of blade bending stiffness, see also figure 6.2.

5.4 Cost of Energy versus Rotor Speed

Several configurations, with differences in nominal rotor speed, have been investigated. Although the blade chord for these configurations is not consistently related to the nominal speed, the cost of energy is plotted versus the nominal speed in the following graph. For all configurations the twist is optimised unless mentioned. The control algorithm for configurations with a higher nominal speed is not adapted.

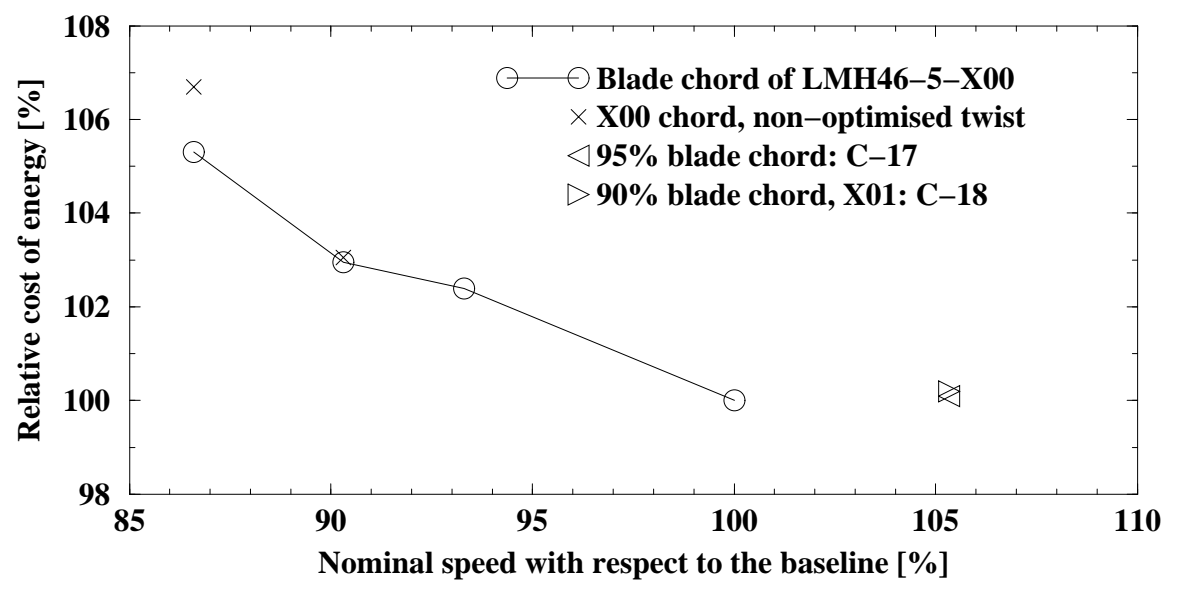


Figure 5.4 Estimated cost of energy versus rotor speed

In fact figure 5.4 shows:

- 1. Optimising the twist does not always pay;
- 2. For the given chord, the 'baseline' nominal speed looks the most cost effective;
- 3. Increasing the nominal speed Ω is not useful if the chord is not scaled with Ω^{-2} .

Regarding the latter two items, this investigation would be more fruitful if (at least) four configurations are analysed for which the chord is scaled with Ω^{-2} , see the relations in appendix C. Here also the blade twist should be optimised and the controller settings adapted.

5.5 Cost of Energy versus Effective Solidity

In figure 4.3 the energy production is plotted versus the product of chord and rotor speed squared, here called 'effective solidity'. This 'effective solidity' indicates how the blade chord is related to the chord for maximum energy capture, see appendix C. Because for different configurations the energy yield appears to be a continuous function of the 'effective solidity' the cost of energy is plotted versus this parameter in figure 5.5. Also here only the configurations with an optimised twist and with the same airfoils as for the baseline configuration are included. The geometry for which the program BOT gives a maximum energy capture will have an 'effective solidity' of 127.6% compared to the baseline.

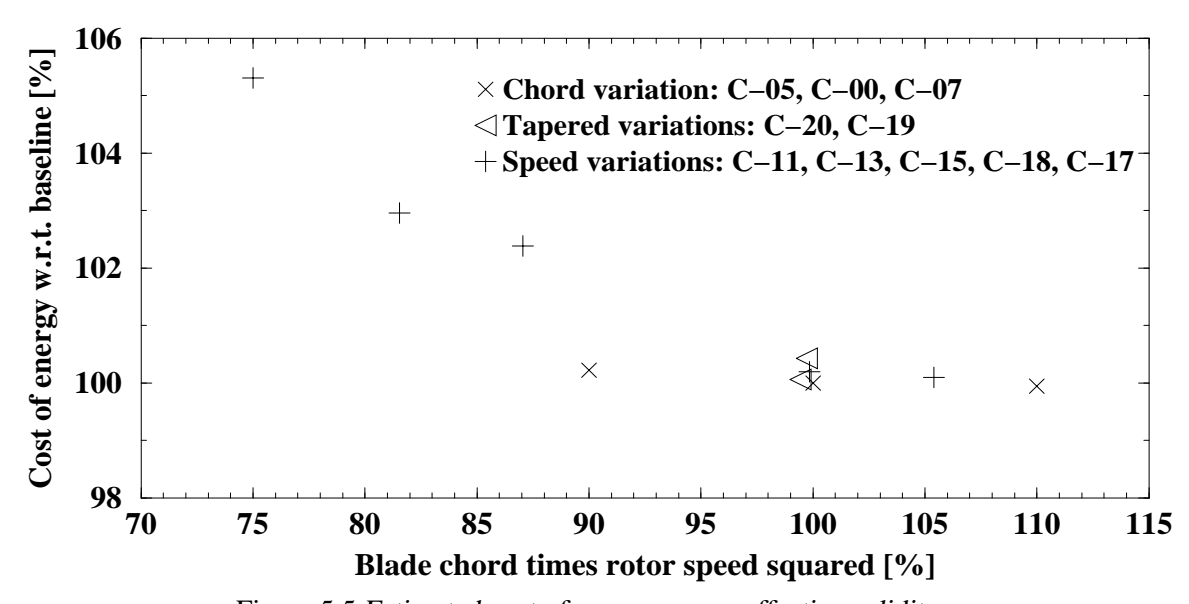


Figure 5.5 Estimated cost of energy versus effective solidity

Because of the strong nonlinear effects in the calculation of the dynamic load set, the points in this graph have a lot of scatter. Still a clear trend can be seen: "The cost-of-energy increases with decreasing relative blade chord or nominal rotor speed."

6. INFLUENCE OF STRUCTURAL BLADE PROPERTIES

Most of the configurations investigated here have variations in the aerodynamic properties. Especially for the 'slender' or 'wide' configurations *C-04* to *C-09* with blade chord variations, it the stiffness properties were expected to be adjusted as was done for configuration *C-06* and *C-08*.

6.1 Influence of Bending Stiffness

In order to evaluate the influence of the blade bending stiffness the dynamic loads are calculated for normal operation at 12m/s stochastic wind, which gives relatively large fatigue loads and also rather large extreme production loads. In these calculations the blade bending stiffnesses have values that are 65.6%, 72.9%, 81%, 90%, 100%, 110%, 121%, 133.1% and 146.4% of the stiffness of the LMH46-5-X00 rotor blade. Because the aerodynamic design of the LMH46-5-X60 rotor blade will be the basis for further design work (configuration *C-21*) these calculations are performed for this rotor blade. The calculated eigen-frequencies and the blade root bending moments (divided by the value for the 'baseline': **100%**) are listed in the following table.

Stiff-	Edge	Flat	Lock	Extreme	Edge moment		Flat moment	
ness	freq.	freq.	number	root mom	fat.equiv.	std.dev.	fat.equiv.	std.dev.
65.6%	1.047	0.8107	8.643	-7.07%	-1.53%	+1.14%	-3.25%	-2.31%
72.9%	1.099	0.8463	8.282	-5.98%	-3.48%	+0.34%	-4.85%	-1.80%
81.0%	1.154	0.8840	7.930	-3.87%	-2.07%	+0.17%	-3.59%	-1.16%
90.0%	1.211	0.9239	7.587	-4.76%	-0.40%	+0.14%	-2.03%	+0.17%
100%	1.271	0.9661	7.254	+0.0%	+0.0%	+0.0%	+0.0%	+0.0%
110%	1.328	1.0063	6.962	-3.48%	-1.18%	-0.39%	-1.50%	-0.43%
121%	1.387	1.0484	6.679	+2.23%	-2.23%	-0.75%	+0.13%	+0.52%
133.1%	1.449	1.0926	6.404	+2.90%	-4.50%	-1.48%	-0.34%	+0.21%
146.4%	1.512	1.1388	6.139	+2.37%	-4.19%	-1.52%	+2.09%	+1.81%

Here the extreme and fatigue blade root moments are the values for all three blades. The Lock number is a dimensionless property that relates the aerodynamic loads to the load variations from structural vibrations. A high Lock number indicates a high aerodynamic damping (in stall it may be a high aerodynamic instability) and a high sensitivity to gusts.

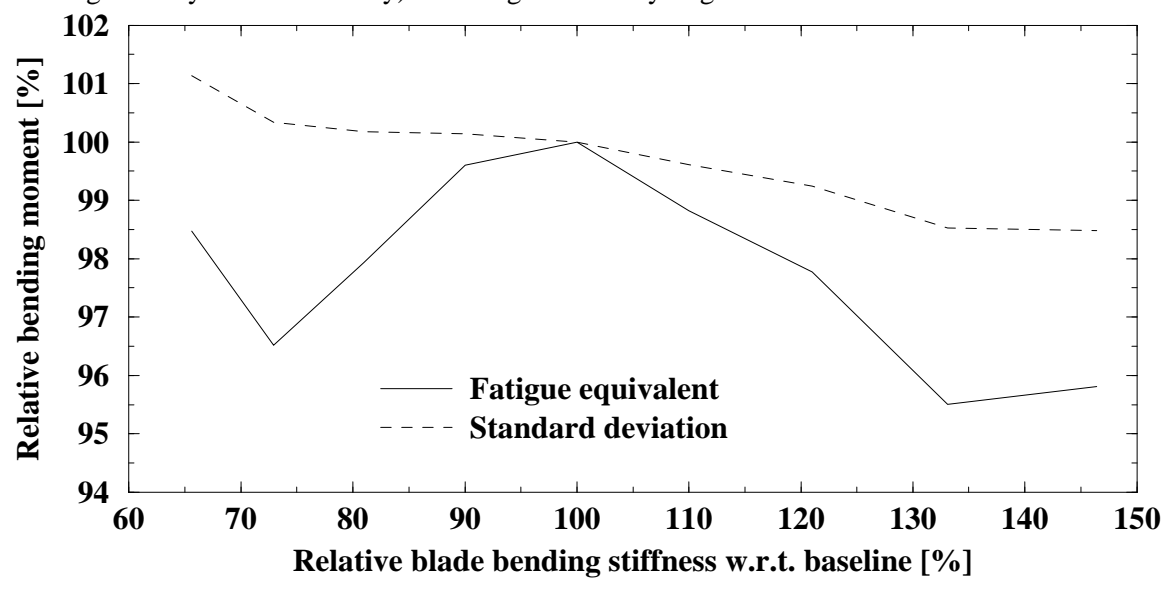


Figure 6.1 Edgewise blade root moments

The fatigue equivalent edgewise moments (figure 6.1) show a distinct maximum for the stiffness of the X00 blade. This is probably caused by the 5P resonance at a rotor speed of 15.24rpm (the nominal speed is 14.92rpm).

The fatigue equivalent flatwise moments (figure 6.2) show a small increase for increasing stiffness, which can simply be explained with the fact that for soft blades the larger deformations give a stronger effect from the centrifugal loads.

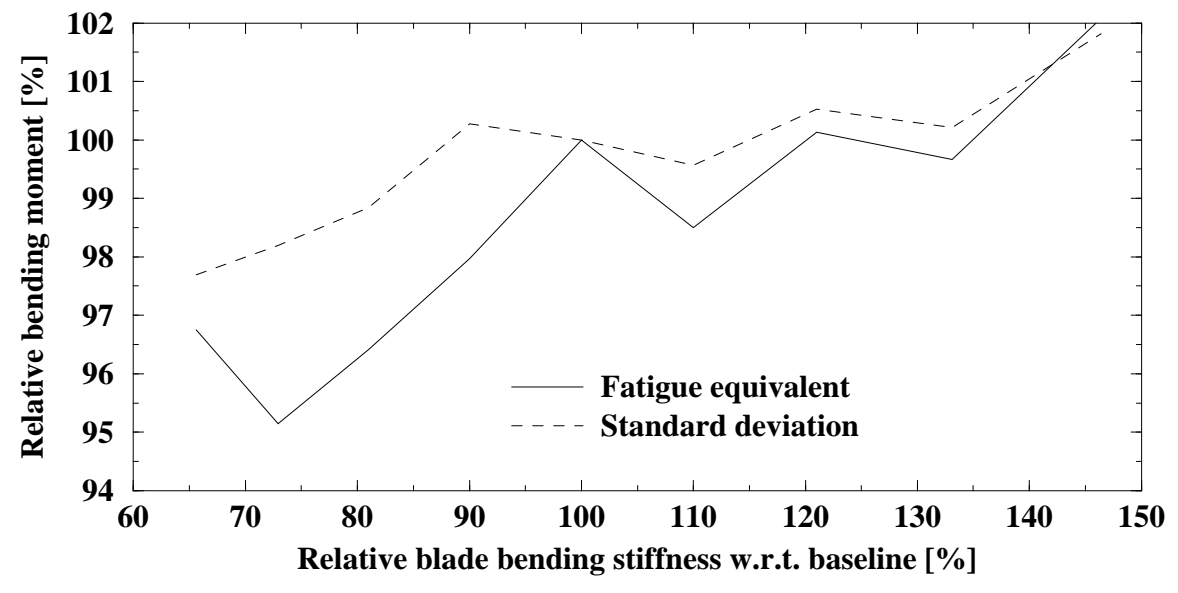


Figure 6.2 Flatwise blade root moments

Especially from figure 6.2 with the flatwise bending moments it follows that at least four values of the blade bending stiffness (or any other parameter) are needed to distinguish a linear trend from a second-order trend and from the scatter in the results.

Sometimes the 'Standard deviation' of the blade bending moments is used as a fast estimate of the fatigue loading. To show the correlation between 'standard deviation' and fatigue equivalent load cycles, both are included in the table and in figure 6.1 and 6.2.

6.2 Influence of Relative Thickness

For a given blade geometry (chord and twist) one can still vary the relative thicknesses. This does not only affect the aerodynamic drag of the airfoils but it also has consequences for the structural properties. Assuming that the flatwise design loads are proportional to the largest pressure on the blade surface, the design bending moment distribution is independent of the relative airfoil thickness. For a given chord and a given flatwise design bending strength of the thin-walled blade cross section, the wall thickness varies with the inverse of the airfoil thickness. This means that the blade mass distribution is inversely proportional to the thickness while the flatwise bending stiffness is linearly related to the thickness.

Since for smaller airfoil thickness, more material is added to obtain sufficient flatwise bending strength, this will not be in the nose or tail of the airfoil. As a result, the edgewise stiffness increases less than linearly with wall thickness. For this reason, in the investigation performed here the edgewise stiffness is assumed to be proportional to the square root of the wall thickness.

Calculations are performed of the dynamic response for normal operation at 12m/s stochastic wind (just above nominal) for a relative blade thickness that is 65.6%, 72.9%, 81%, 90%, 100% and 110% of the thickness of the LMH46-5-X60 blade. These mass and stiffness variations are only applied for the aerodynamic part of the blade. For simplicity the geometry and the airfoil distribution will be the same as for the LMH46-5-X60 blades such that the same twist distribution and the same aerodynamic rotor characteristics apply. Because for most of these thickness variations (except for the 110% thickness) the rotor inertia is larger, the energy buffering capacity of the rotor (flywheel effect) will be larger such that there is no urgent need to adapt the control algorithm.

The calculated eigen-frequencies and the blade root bending moments are listed in the following table.

Airfoil Rotor	Edge Flat Lock	Extreme	Edge moment	Flat moment
thickn. inertia	freq. freq. number	root mom.	fat.equiv. std.dev.	fat.equiv. std.dev.
65.6% 20.49e+6	1.129 0.685 6.670	+8.25%	+45.69% +53.20%	+10.20% +8.83%
72.9% 18.44e+6	1.165 0.743 6.849	+1.05%	+37.53% +38.07%	+2.28% +5.43%
81.0% 16.60e+6	1.201 0.809 7.005	+1.33%	+21.64% +23.70%	+1.83% +3.00%
90.0% 14.95e+6	1.236 0.883 7.139	-0.002%	+11.19% +11.27%	+0.94% +1.10%
100% 13.46e+6	1.271 0.966 7.254	+0.0%	+0.0% +0.0%	+0.0% +0.0%
110% 12.24e+6	1.291 1.055 7.331	-2.91%	-8.67% -9.13%	-0.61% -1.73%

Here the extreme and fatigue blade root moments are the values for all three blades. From the table and figures 6.3 and 6.4 it follows that the fatigue equivalent cycles and the standard deviation of the edgewise blade root moment is directly (linearly) related to the rotor inertia (inverse of the relative thickness). The extreme root moment as well as the standard deviation of the flatwise bending moment shows a small but direct relation to the blade mass distribution.

Although these results show continuous trends, they have limited value since they are calculated for a single load case only while each variation is calculated with the same airfoil distribution and control algorithm.

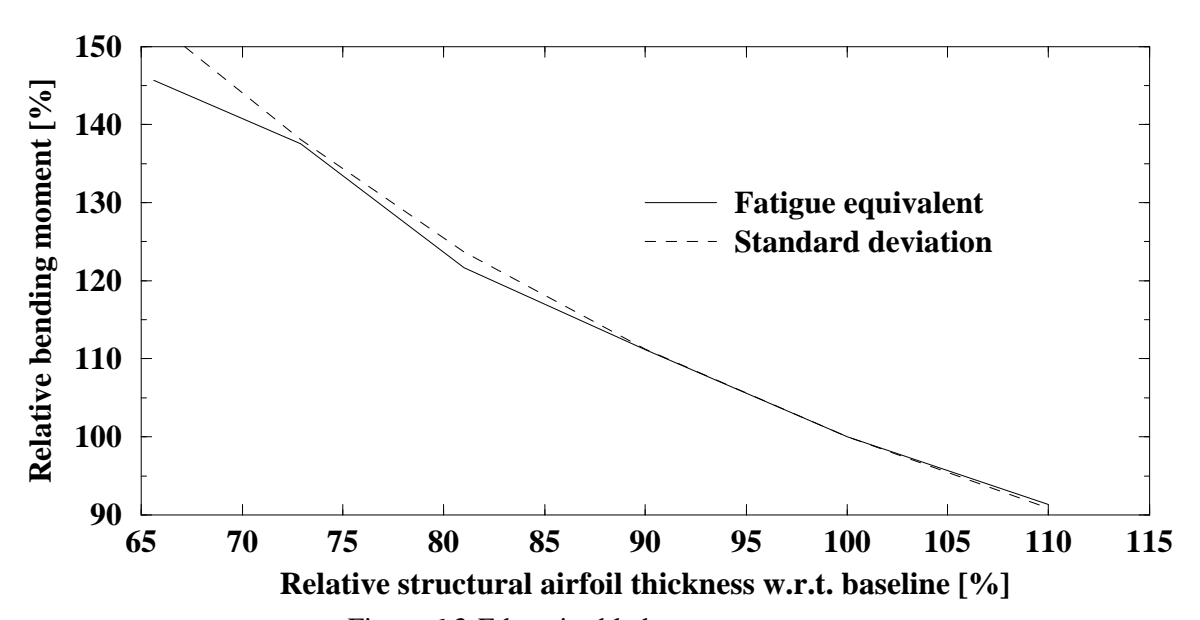


Figure 6.3 Edgewise blade root moments

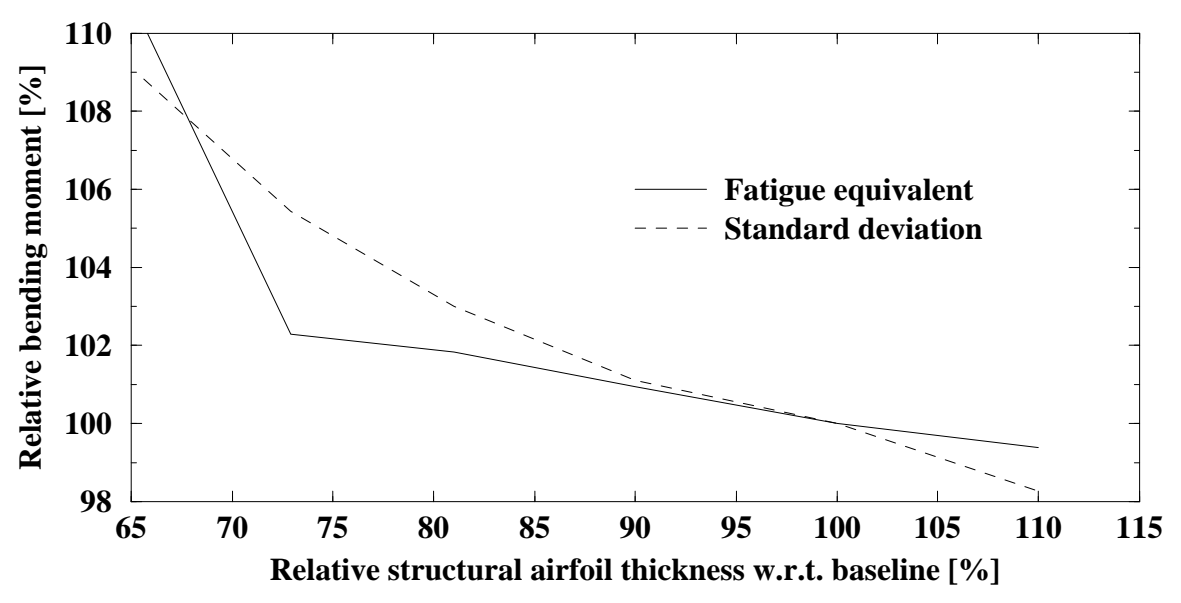


Figure 6.4 Flatwise blade root moments

7. CONCLUSIONS

Not all of the following conclusions are directly based on the results of the calculations, but also based on knowledge and insight obtained during this sensitivity analysis.

7.1 General

- **1.1 Use 4+ parameter values** A sensitivity analysis on basis of dynamic load set calculations (including control) requires at least 4 parameter values (= load sets) to assess a linear relation. With less parameter values (see e.g. figure 6.2) it is not possible to judge whether deviations from a linear trend are due to a second order relation or due to scatter from the non-linear calculations.
- **1.2 Define meaningful parameters** Parameter sensitivity studies are performed in which only one property (such as blade chord) is varied while other directly-related properties (such as rotor speed) remain constant. In this approach (considering that one uses enough parameter variations to assess a clear relation) one may likely conclude that the parameter value for the baseline configuration is close to the optimum.
 - Unfortunately in many of the configurations analysed here, only one single property is varied, except for the configuration *C-18* where the product of rotor-speed squared and blade chord is kept the same as for configuration *C-00*. This product is a measure for the here called 'effective solidity', and might be a property to optimise, or to keep constant when varying other parameters.
- **1.3 Cost dependencies are approximations** The component costs are expressed in terms of a limited set of fatigue and extreme loads. The influence of rotor mass for example is not included because this mass is assumed constant in the calculation models used for this study. From the structural design this mass is directly related to the blade loads. Since the sideways tower motion has little aerodynamic damping, the sideways bending moments may strongly depend on the rotor configuration. Because several of those dependencies are not included, the cost of energy presented in chapter 5 is also for this reason a rough estimate.

7.2 Load set Calculations

- **2.1 Turbulence contains energy** The smaller predicted energy capture for the "SEA" climate with lower turbulence intensity is caused by the smaller amount of energy present in the wind.
- **2.2** Use larger wind intervals above nominal For the fatigue load set, the variations with wind speed of the average power and of the extreme and fatigue loads is strong for wind velocities up to 130% of the nominal value while the variations are very small above this wind velocity. From these observations, and knowing that for offshore wind turbines different wave loadings (e.g. wave directions) should be combined with different wind loadings, it follows that above 130% of the nominal wind speed, the wind interval can be 2m/s instead of 1m/s. For the governing turbine this reduces the amount of production load sets from 21 to 17.
- **2.3 Calculate both neg. and pos. misalignment** The extreme blade loads are in most cases predicted for load cases with a negative misalignment while the minimum tower clearance is predicted for load cases with a positive misalignment.
- **2.4 Extreme loads depend on control settings** For IEC load case DLC1.3 ('Extreme Coherent gust and Direction change', ECD) (file 131) the reaction of the pitch control algorithm on this ECD can result in extreme blade moments. Modifications of the control algorithm aiming to reduce the calculated extreme loads do not guarantee that the loads of real-life gusts will be smaller, especially because this transient reaction is also dependent on the value of the ambient wind speed and the phase between the gust and the direction change.

2.5 Stand-still loads depend on yaw friction The calculated dynamic loads for a parked rotor are strongly dependent on the yaw response, which is directly influenced by the yaw friction. A small yaw friction results in a high sensitivity to wind speed and wind shear variations and thus to many yaw fluctuations. A high yaw friction gives a delay in yaw response which means that if the turbine follows the wind, it may accelerate strong in yaw. For the load set calculations reported here, the yaw friction has been chosen such that a parked rotor at high wind does not give the largest loads except for some configurations. This however is not allowed for an existing yaw system, which was not fully specified.

7.3 Aerodynamic Optimisation

- **3.1 Exclude tip in finding optimum pitch** In the optimisation of the blade twist for maximum energy yield, the partial load pitch angle is also included. Because the 'aero-acoustic' shaped tip aims at a uniform distribution of the trailing vorticity, the orientation of this tip should not be included in optimising the pitch angle. In the calculations with PHATAS the blade-twist (without tip) is increased/decreased such that the optimum pitch setting angle is near 0deg.
- **3.2 Avoid angle-of-attack larger than optimum-** Because of the different airfoils used, the optimum twist as calculated with BOT is not always a continuous function of radius. This is a result of the different angles of attack for maximum c_1/c_d for each of the airfoils. Although smoothing of the twist may give loss of energy, it will in practise not be so serious as long as the smoothed twist has only local differences compared to the theoretical optimum twist. Knowing that for the smoothed twist the lift distribution is not continuous, its spanwise derivative will give some trailing vorticity. This trailing vorticity distribution gives a reduction of induced velocity at the parts with a lower lift and an increased induced velocity at the parts with a higher lift. Thanks to this effect the loss in energy capture is not so bad as calculated following Blade Element Momentum theory.
- 3.3 Reduce angle-of-attack slightly for moisture or turbulence Optimisation of the blade chord and twist leads to an equilibrium of induced velocity and the aerodynamic loads near an angle of attack for maximum c_1/c_d . For a slightly smaller angle of attack, this lift-drag ratio is not much different while for a slightly higher angle of attack this ratio may reduce because of the progressive increase of drag. Because of this effect an optimum blade will perform less for a stronger variation of the airfoil angle of attack which is the case in turbulent flow. The effects for turbulence and/or vertical shear may be included in a simple way by decreasing the Weibull-shape factor, and thus giving an artificial increased variation in angle of attack. One should also realise that an increase of the drag coefficient for small angles of attack due to moisture (roughness) on the blades may be a serious factor of influence.
- **3.4 Spline optimum geometry with appropriate functions** The optimum twist appears to have a varying shape that is not wanted from structural, manufacturing or cosmetic point of view. It was realised that a too strong twist variation ('cork-screw' shape) towards the root is not wanted for structural reasons while it also gives a blade shape for which the flow will be far from 2-dimensional. An optimisation in which the twist is constructed from a finite number of smooth functions can ensure a smooth chord and twist.

A suggestion for these functions is: $a_0/r + \Theta_{tw} + a_1 r + a_2 r^2$.

Here the term a_0/r is added because for a blade with one single airfoil operating at constant lambda, the optimum chord and twist have an 1/r shape. After multiplication with the radius (which can be seen as a weighting function for the amount of rotor swept area) these functions form in fact a third-order polynomial. Using the radius as weighting function in fitting the twist accounts for the fact that the outer part of the blade contributes more to the energy capture. A higher-order polynomial function is not recommended because this introduces stronger twist-variations towards the root and the tip.

3.5 Increase chord where angle-of-attack tends to be too high When smoothing the optimised twist one should avoid strong twist reductions (higher a.o.a.) because this may lead to a local increased drag coefficient. If smoothing the geometry leads to a local decreased twist value (increased a.o.a.), one may better increase the chord slightly instead of decrease the twist.

7.4 Aerodynamic Parameter Variations

- **4.1 DU 96-W-180 vs. NACA64-618** The configuration *C-02* with the DU 96-W-180 airfoil at the outer part of the blade gives loads that differ significantly from the loads for the baseline configuration *C-00*. This directly reflects the differences in aerodynamic coefficients, see figure 2.1. The different aerodynamic coefficients for the NACA64-618 and the DU 96-W-180 airfoils may arise from the fact that they are not measured in the same wind tunnel.
- **4.2 Dependency on** ' $c \Omega^2$ ' In section 4.1 and appendix B it is shown that, using the product of chord and nominal speed squared ('effective solidity') as parameter, the annual energy capture shows a continuous second-order trend, which can also be read in appendix C. For the annual power from the calculations with BOT, the annual energy looks to have its maximum at a smaller chord value than from the dynamic load set calculated with PHATAS. For normal operation with 'average' turbulence and shear, the calculated energy capture shows a trend between that calculated from a stationary PV curve and that integrated from the dynamic load set, see appendix B.
- **4.3 More slender makes sense** The slenderness of the rotor blades show to have a direct effect on the extreme moments as well as on the fatigue loads. The configurations *C-06* and *C-08* with slender and wide blades of which the stiffness is adapted give extreme moments and fatigue equivalent moments that increase with the chord.
- **4.4 Tapered chord** Configurations *C-19* and *C-20* (tapered modifications of blade X00) show a small increase in energy capture and a reduction in dynamic and extreme loads of several percent, except for the extreme tower base bending moments. For the blade loads the tapered configurations show to be favourable, which also holds for the LMH46-5-X60 rotor blades.
- **4.5 Higher** Ω The "fast and slender" configurations *C-17* and *C-18* give a somewhat higher annual energy capture, because a higher tip-speed ratio ($\lambda = 7.9$) gives smaller tip losses.
- **4.6 LMH46-5-X60** For configuration C-21 with the LMH46-5-X60 blade the structural loads and finally the cost of energy seem not to be the most favourable. This however is strongly influenced by the fact that airfoil coefficients for a Reynolds number of $7 \cdot 10^6$ are used, of which the maximum lift coefficients are higher. This is shown by the similar load set for the LMH46-5-X00 rotor blades with Re = $7 \cdot 10^6$ airfoil coefficients, configuration C-22. The annual energy capture for configuration C-21 is smaller than for configuration C-22 which is caused by the fact that the twist is not optimised after selection of the Re = $7 \cdot 10^6$ airfoil coefficients, and caused by the fact that for the tapered geometry the blade shape differs more from the aerodynamic optimum.
- **4.7 Edge vibrations in blade tip** For configuration *C-02* and *C-19* it was found (after a remark from R. v.d. Berg) that the blade with a negative pitch error, giving a larger angle of attack, can be sensitive for edgewise vibrations. Here the negative pitch error was assigned to blade 3. This will be investigated starting with some scoping calculations.

7.5 Cost of Energy

- **5.1 Strong dependency on turbine settings** The extreme and/or fatigue loads, e.g. when idling at the extreme wind, strongly depend on the turbine settings such as yaw friction or brake pitch rate. If these settings are not adapted (optimised) for each turbine they may give occasional high loadings and thus result in an unfortunate high cost of energy.
- **5.2 Sub-optimal 'effective solidity'** From figure 5.4 it follows that an 'effective solidity' (product of chord times nominal speed squared) of around 80% of the value for maximum yield, gives the smallest cost of energy.

7.6 Structural Parameter Variations

- **6.1 Tower damping** An increased damping in the tower reduces at least the dynamic loads in the tower.
- **6.2 Shaft torsion** Modelling of shaft torsion gives a direct increase in the in-plane blade loads in sideways tower moments. For this sensitivity analysis it was thought that the drive train dynamic properties were not specified well enough to model its dynamics reasonably.
- **6.3 Pre-bend modelling** The dynamic loads calculated for configuration *C-25* with the straight rotor blades show a small reduction in operational and in overall extreme moments compared to the baseline configuration *C-00*. Here one should realise that the pre-bend is modelled as an upwind cone angle, except for configuration *C-21* to *C-24* and *C-26*.
- **6.4 Stiffness variation** Variation of the blade bending stiffness shows no clear trend in the blade edgewise moments for operation at 12m/s, because these moments are partly due to the deterministic gravity loads. The 5P resonance for the baseline stiffness can still be recognised in figure 6.1.
 - Variation of the blade bending stiffness shows that the flatwise moments are roughly proportional to the flatwise stiffness. This can be explained with the centrifugal stiffening which gives a stronger restoring effect for larger blade flapping deformations.
- **6.5 Thickness variation** The structural effects for variation in blade thickness (airfoil thickness) show to have a direct effect on the standard deviation of the blade bending moments. The larger blade mass for the thinner blades gives a direct increase in the edgewise moment variations and a smaller but also continuous increase in flatwise moment variations.

REFERENCES

[1] Bot. E.;

'Blade Optimisation Tool'.

Development (1999-2000) by E. Bot of ECN Wind Energy.

[2] Dobbe, T., Bensoussan R. and van den Berg, R.;

'Concept design of a 3MW offshore rotor blade, LMH46-5-X00'.

OD.00.031, rev.1, June 16, 2000.

[3] Dobbe, T., Bensoussan R. and van den Berg, R.;

'Concept design of a 3MW offshore rotor blade, LMH46-5-X01'.

OD.00.033, rev.1, July 6, 2000.

[4] Dobbe, T., Bensoussan R. and van den Berg, R.;

'Concept design of a 3MW offshore rotor blade, LMH46-5-X02'.

OD.00.034, rev.1, July 6, 2000.

[5] ESDU;

'Mean fluid forces and moments on cylindrical structures:

Polygonal sections with rounded corners including elliptical shapes'.

Engineering Sciences Data Item Number 79026, ISBN 0 85679 274 8, 1979,

Specialised Printing Services Limited, 7-9 Charlotte Street London W1P 2ES.

[6] Germanischer Lloyd;

'Vorschriften und Richtlinien Nicht Maritime Technik,

Teil 1 - Richtlinie für die Zertifizierung von Windenergieanlagen'.

Ausgabe 1999.

[7] Goezinne F. and Sonderby, O.;

'3MW turbine data for blade optimisation'.

Nr. 001-FG-R0067, rev.21, June 2000

[8] van der Hooft, E.L.;

'DOWEC Blade pitch control algorithms for blade optimisation purposes'.

ECN-CX--00-083, Petten, The Netherlands, February 2001

[9] International Electrotechnical Commission;

'INTERNATIONAL STANDARD, Wind turbine generator systems -

Part 1: Safety requirements'. IEC 61400-1 Second edition 1999-2.

[10] Kooij, J.F., Bensoussan R, and van den Berg, R.;

'Concept design of a 3MW offshore rotor blade, LMH46-5-X00'.

OD.00.031, rev.1, June 16, 2000.

[11] Lindenburg C, and Schepers J.G.;

'PHATAS-IV AEROELASTIC MODELLING'.

ECN-CX--00-027, Petten, April 2001.

[12] Lindenburg, C.;

'STALL COEFFICIENTS, Release "DEC-2000". ECN-Wind Memo-00-031, February 2001.

[13] Lindenburg, C. and Hendriks H.B.;

'LOAD SET FOR NM3000 - LMH46-5-X00, Dynamic Loads calculated with PHATAS-IV for the 3MW NEG Micon wind turbine with "baseline" LMH46-5 blades'. ECN-C--00-077, ECN, Petten, May 2001.

[14] Rosen, A. and Sheinmann Y.;

(Faculty of Aerospace Engineering, Technion, Israel Institute of Technology, Haifa 32000) 'The average output of a wind turbine in a turbulent wind'.

In Journal of Wind Engineering and Industrial Aerodynamics, Vol.51, pp.287-302, 1994.

APPENDIX A. OPTIMUM BLADE GEOMETRY

A.1 Blade Chord

Chord for maximum yield

In the past the aerodynamic design of rotor blades for wind turbines aimed at a maximum annual energy capture. For this purpose aerodynamic optimisation tools have been developed such as the ECN programme BOT, 'Blade Optimisation Tool'.

Smaller chord to reduce design loads

With the increasing dimension of wind turbines it is realised that the structural loads are an increasingly important factor that is of influence on the cost of energy. For this reason many modern wind turbines of medium size and larger have a blade chord that is smaller than the chord needed for maximum energy capture. The improvement for more slender blades is based on the fact that near the "aerodynamic optimum" the annual energy capture varies only slightly with variation in blade chord while the blade loads (due to gusts or parking at strong wind) vary linearly with blade chord.

For this reason some configurations with different blade chord were investigated in the sensitivity study reported here.

Tapering the chord to reduce blade root moments

Looking in more detail one can imagine that loads on the blade tip have a relatively strong contribution to the structural loads in the blade compared to loads in the blade root. This has shown to be the case with tapered variations on the blade chord, see section 4.3.5.

Suggestion for tailoring chord distribution to minimise structural shaft loads

For large size wind turbines the cost of the nacelle and of the support structure is a large fraction of the total turbine cost so that the asymmetric loads from the rotor on the support structure are important. This is especially true for offshore wind turbines. A load/energy efficient rotor blade for large turbines should be designed such that each section in the blade has the same ratio between blade-chord-derivatives of:

- 1. annual energy yield,
- 2. asymmetric rotor shaft loads from yaw misalignment, gusts or wind shear.

The use of DU 96-W-180 airfoils (with lower maximum lift) for the blade tip was in fact based on the same considerations drawn here for finding the blade geometry.

While performing this aerodynamic sensitivity study the author realised that designing blades based on this procedure is possible with the present state-of-the-art of rotor aerodynamics and of the design programs.

A.2 Blade Twist

In the sensitivity studies reported here the blade twist has been optimised towards maximum annual energy capture for most of the configurations. From a straightforward point of view, an energy-optimised blade will give a lower cost of energy than a non-optimised blade.

A non-optimised twist is not always as bad as calculated as long as the deviations with respect to the optimised twist are local, i.e. over a span with the dimension of the chord.

Although in chapter 5 this has shown to be true, it also appears that the configuration C-10, with non-optimised-twist, give somewhat smaller extreme structural loads than the similar configuration C-11 with optimised twist. This however may be caused by scatter.

The fatigue loads on the rotor blades are directly a result from varying aerodynamic forces on the airfoil sections. On this basis TU-Delft developed some airfoils that have a reduced maximum lift coefficient such that the load variations are smaller, see e.g. chapter 2. In addition to the selection of airfoils one may also vary the blade twist such that variations in relative wind velocity give small variations in aerodynamic loads. For this purpose a real strategy is not yet formulated. Basically this is the same design philosophy for passive stall regulated wind turbines.

A.3 Optimised Parametric Geometry

For a rotor blade in which different airfoils are used, the optimised geometry (e.g. for maximum yield) may show non-continuous variations in chord and twist in the areas with airfoil transitions. An irregular chord- and twist distribution will not be applied in a large rotor blade because:

- It looks bad;
- The aerodynamic flow is not 2-dimensional;
- A geometry that is not smooth (quasi-prismatic) in spanwise direction may give secondary loads and/or stress concentrations;
- If the spanwise load distribution has local deviations from the optimum (caused by 'smoothing') then the wake structure behind the blades contains tangential vorticity. This tangential ('trailing') vorticity induces a variation on the local inflow distribution that compensates partly the discontinuities in load distribution.

In short terms: A geometry that is not optimum on basis of blade element momentum theory will still be closer to the optimum design because of the influence of the local wake structure.

The last argument (for which deviations from the optimum are accepted) is especially valid for local deviations. Combining all arguments one may conclude that an optimised chord and twist distribution that is constructed from a small set of smooth functions is practical and does in practise not give much loss compared to the theoretical optimum.

The functions for the chord and twist should be smooth and chosen such that with a few functions the optimum can be approached reasonably. For this last requirement, a function proportional to the inverse of the radius 1/r fits the optimum design of a rotor with a single airfoil and running at constant tip-speed ratio. This holds for both the chord and twist. In addition to this function the pitch angle is in fact the 'constant term' of the functions. For finding a better optimum it is suggested to use also functions proportional to the radius r and to the radius squared r^2 . Higher order polynomial functions are *not* recommended because they give increasing second-order spanwise derivatives towards the blade tip, which not only look ugly but also are bad because the aerodynamic properties show less variations towards the blade tip. The suggested function to describe the blade geometry (here twist) is thus: $\Theta(r) = \Theta_{\text{pitch}} + c_0/r + c_1 r + c_2 r^2$.

For smoothing the geometrical properties of a rotor blade while conserving its aerodynamic properties, it is finally recommended to use a weighting function that is proportional to the swept-area of the blade sections, which is simply the radius r. Multiplying the (suggested) basis-functions for the blade geometry with this weighting-function r simply gives a third-order polynomial which may be more easy to handle numerically. The result should finally be divided by the radius. If constraints (such as max-chord) are active, then these should also be applied after they are multiplied with the radius r.

APPENDIX B. CALCULATION METHODS FOR ANNUAL YIELD

From figure 4.3 it follows that the relation between 'effective solidity' and calculated annual yield depends clearly on the calculation of the power curve. If the annual yield is used to compare different configurations on basis of (in this report) cost of energy, this may be influenced by the analysis tool. This holds in particular for optimisation processes in which the calculated energy production is involved. In this report the cost of energy is calculated with the annual yield integrated from the dynamic load set. The most realistic cost of energy would be obtained if the annual yield is calculated for less severe load conditions because the IEC conditions for dynamic-load calculations include some conservatism.

In this appendix a comparison between several calculation methods for the annual yield is reported. This comparison is done for the configurations that have only chord-variations and/or rotor-speed variations that all have the same airfoils and an optimised twist. This comparison is done on basis of the power curves calculated with different programmes/conditions.

Program	Turbine	Shear	Yaw	Pitch	Turbulence
and method	geometry	exponent	error	error	intensity
BOT, optimisation	none	0.0	0.0	0.0	0.0
PHATAS, PV-curve	All	1/7	0.0	0.3deg	0.0
PHATAS, dynamic loads	All	1/7	5.0deg	0.3deg	12%
PHATAS, IEC load set	All	0.2	10.0deg	0.5deg	16%

The yield from 'PHATAS, dynamic loads' is introduced here as the most realistic approach of the annual energy capture. The vertical shear exponent 1/7 is for the 'standard atmosphere'. If the annual yield for each of the calculation methods is scaled with the value for the 'baseline' configuration C-00, the result is:

	Effective	BOT	PHATAS	Dynamic	IEC
Configuration	solidity	optim.	PV-curve	loads	load-set
C-00: LMH46-5-X00 "baseline"	100%	100%	100%	100%	100%
C-05: X01: 90% slender chord	90.00%	-0.739%	-1.071%	-1.702%	-2.094%
C-07: X02: 110% wide chord	110.00%	+0.241%	+0.168%	+0.238%	+0.786%
C-11: X00, 86.6% sub-opt. speed	75.00%	-2.745%	-3.440%	-4.414%	-5.964%
C-13: X00, 90.3% sub-opt. speed	81.54%	-1.578%	-1.773%	-2.625%	-4.051%
C-15: X00, 93.3% sub-opt. speed	87.05%	-0.925%	-1.079%	-1.774%	-3.107%
C-17: Tip speed 79m/s, 95% chord	105.40%	+0.365%	+0.159%	+0.436%	+0.383%

In figure B.1 these calculated values for annual yield are plotted as continuous functions against the 'effective solidity'. The annual yield calculated with each of the methods shows a clear (smooth) second-order dependency with the 'effective solidity'. This trend however is not the same for each of the calculation methods but gives a stronger linear dependency if more turbulence is included in the analysis method. This means among others that the power-curve calculation in an optimisation process can seriously influence the resulting optimum geometry.

From figure B.1 it can be concluded that the (calculated) geometry for maximum yield has a larger solidity if turbulence is included. This means that the maximum-yield geometry as calculated with BOT has a smaller chord than the real maximum yield geometry.

The cause for this 'turbulence dependency' is that for a constant wind loading, the twist of the blade-geometry for maximum yield is such that in partial-load operation, the angle-of-attack is close to the valued for maximum $c_{\rm l}/c_{\rm d}$. For turbulent wind, the angle of attack varies around

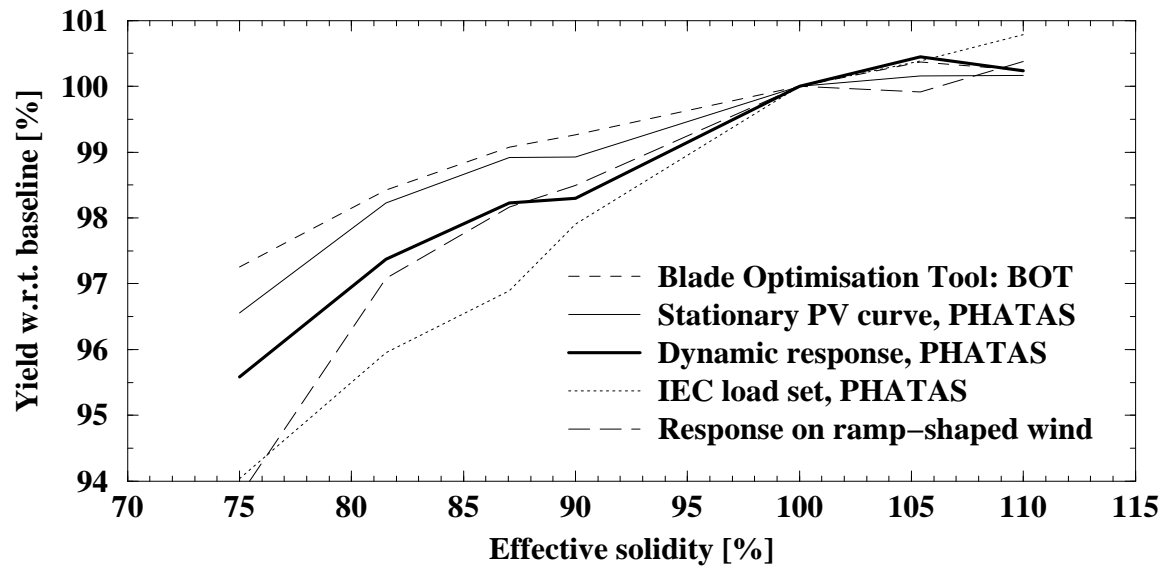


Figure B.1 Annual yield v.s. 'effective solidity'

this 'maximum c_1/c_d ' value which means that not only the maximum c_1/c_d -value determines the performance, but also the values at neighbouring angles of attack. For the NACA64-618 airfoil,

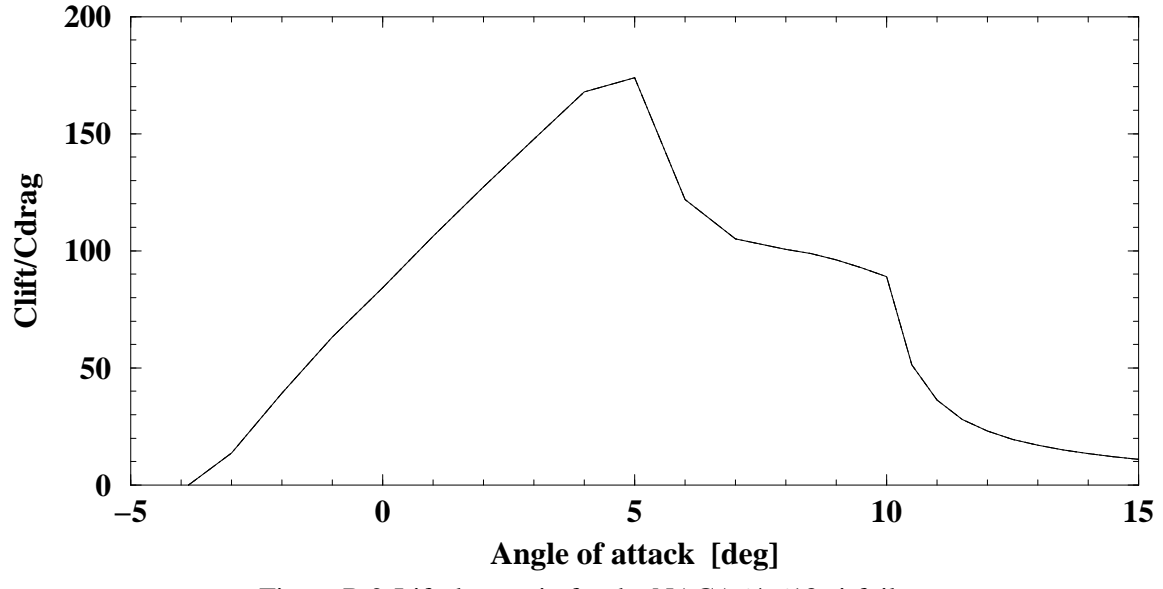


Figure B.2 Lift-drag ratio for the NACA64-618 airfoil

which has the largest swept area of the LMH46-5-X00 blade, the c_1/c_d ratio is plotted in figure B.2 as function of angle of attack. Figure B.2 clearly shows that starting from the maximum c_1/c_d a 2deg increase in angle of attack gives a far stronger reduction than a 2deg decrease. Knowing that in turbulent wind the angle of attack is continuously varying, the 'turbulent optimum c_1/c_d ' is at a somewhat smaller angle of attack than the stationary optimum. Figure B.3 shows the cost of energy for a turbine following the cost-estimates in chapter 5 and the annual yield from the (12% turbulence) dynamic load calculations. Figure B.3 shows a minimum that is more towards the 'smaller solidity' compared with figure 5.5.

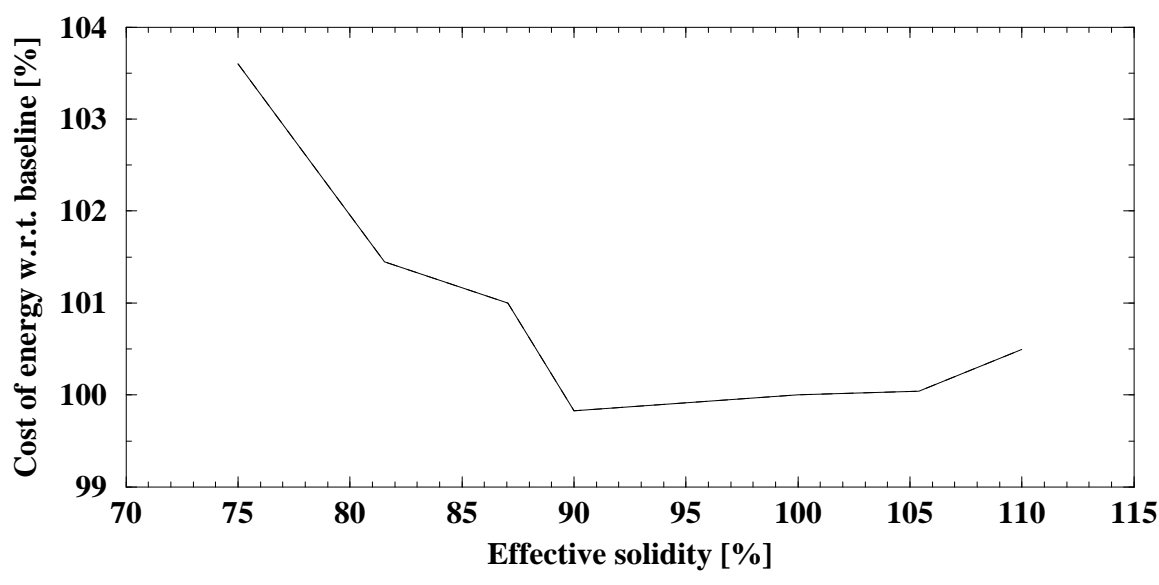


Figure B.3 Estimated cost of energy versus effective solidity

Option for Power Curve Computation

By comparison of the annual yield for different (external) conditions it is shown that the trend in annual yield with effective solidity depends among others on the turbulence. For wind turbines as in this investigation (variable speed, pitch controlled) the discrepancy is caused by the fact that turbulent wind causes variations in blade angle-of-attack, and that the controller is lagging the rotor-averaged wind speed fluctuations.

At this moment it is considered that for optimisation purposes, calculating the dynamic loads during production (which have different conditions as for the IEC load set) is the most realistic approach for the annual yield. Because dynamic load calculations (e.g. up to 120% of the nominal speed) take a lot of time and disk space, it is suggested here to calculate the dynamic response for a slowly increasing and decreasing wind speed. After some attempts the response is calculated for a wind speed that increases with a rate of 0.2m/s/s. The vertical shear is described with an exponent of 0.2 in order to account for the angle-of-attack variations that normally come from turbulence. The yield from this calculation is integrated from the average of the power for the increasing and decreasing wind, of which the result is plotted in figure B.1 (long-dashed line).

From figure B.1 is follows that the resulting trend in annual yield compares better with that from the 'Dynamic response' than if calculated from a stationary PV curve. However, the second derivative in the trend looks a bit too strong while the relation is not as smooth as one would like for optimisation.

APPENDIX C. ROTOR BLADE SCALING RELATIONS

In this report, elementary sensitivity studies are performed to the influence of: chord, nominal speed and taper.

The influence of blade bending stiffness is investigated separately although in reality the bending stiffness is strongly related to design parameters such as blade chord and rotor speed. After all it appeared to be difficult to directly draw clear conclusions from the calculated load sets.

When looking for a cost-efficient rotor blade, one can analyse several variations on basis of calculated load sets, such as reported in this document. Because this approach requires a lot of analysis time and because a thorough investigation may end up in a wide variety of configurations, this implies large effort.

A faster process to obtain an optimised design is possible if the number of parameters of a rotor blade is reduced to a limited set that are really meaningful. Analytical relations are then used as far as possible to express some rotor blade properties in terms of those parameters.

The remaining questions/unknowns, can then be quantified with a limited number of load-set calculations.

In this appendix several properties of a rotor blade are drawn as function of some parameters. The underlying assumptions and expressions are:

- The tip speed ratio is high, such that the rotational velocity dominates the wind speed;
- The blade chord c has the same relative spanwise distribution, which is proportional to (but smaller than) the chord for maximum energy capture c_{max} ;
- From blade cross sections of large rotor blades it is assumed that they include the construction of an I-spar beam, of which the width of the flanges is proportional to the chord while the wall thickness h can be treated as small compared to the airfoil thickness t. This gives for the sectional mass: $\rho \cdot 2ch$, for the flat-bending stiffness: $E \cdot hct^2/2$, and for the edge-bending stiffness: $E \cdot hct^3/6$;
- Because the effect of taper is not included, the bending modes have the same shape;
- The blade wall thickness is dimensioned to carry the aerodynamic loads.

The relation of the loads, stiffnesses and finally the mass of rotor blades with constant tip-speed ratio as function of its dimension/diameter D can be drawn relatively easy.

In the following sections, the diameter, the tip-speed-ratio and the design wind velocity are the parameters. Alternative relations are listed in which the rotor speed is used as parameter instead of the tip-speed ratio.

Relations if Parking Loads are Dimensioning

For stand-still conditions the loads are proportional to the blade surface, the wind velocity squared and to the drag coefficient. For the influence of the drag coefficient, the relation for a flat plate with finite aspect ratio is used: $C_{\rm d}(90)=2.0-0.82\,(1-e^{(-17/{\rm AR})})$.

Here the aspect ratio under consideration is 16, which is about the aspect ratio for the LMH46-5 rotor blade. This gives $C_{\rm d}(90)=1.463$ and $\partial C_{\rm d}/\partial (1/AR)=-4.82=-0.206$ $C_{\rm d}(90)$ AR. Because for other angles of attack this derivative is less strong, it is approximated here as -0.2.

The following table shows the properties of a rotor blade for the case that the wall thickness is dimensioned with the largest wind loading during stand-still (or idling) at the extreme wind $V_{\rm ref}$

	Diameter	Wind	Tip speed	No. of	Rel. chord	Rel. airfoil
Property		speed	ratio λ	Blades	$c/c_{ m max}$	thickn. t/c
Rotor speed Ω	D^{-1}	$V_{ m ave}^{-1}$	λ^1	1	1	1
Rotor area	D^2	1	1	1	1	1
Blade chord <i>c</i>	D^1	1	λ^{-2}	B^{-1}	$(c/c_{ m max})^1$	1
Blade area	D^2	1	λ^{-2}	B^{-1}	$(c/c_{ m max})^1$	1
Aspect ratio	1	1	λ^2	B^1	$(c/c_{ m max})^{-1}$	1
				<u>I</u>	, , , ,	
	Following	properties ar		he wall th		
Bending stiffness/h	D^3	$V_{ m ave}^{0}$	λ^{-6}	B^{-3}	$(c/c_{ m max})^3$	$(t/c)^{2}$
Sectional mass/h	D^1	$V_{ m ave}^{0}$	λ^{-2}	B^{-1}	$(c/c_{ m max})^1$	$(t/c)^{0}$
Total blade mass/h	D^2	$V_{ m ave}^{0}$	λ^{-2}	B^{-1}	$(c/c_{ m max})^1$	$(t/c)^0$
Rotor inertia/h	D^4	$V_{ m ave}^{0}$	λ^{-2}	B^0	$(c/c_{ m max})^1$	$(t/c)^0$
Gravity moment/h	D^3	$V_{ m ave}^{0}$	λ^{-2}	B^{-1}	$(c/c_{ m max})^1$	$(t/c)^0$
Edge. resistance/h	D^2	$V_{ m ave}^{0}$	λ^{-4}	B^{-2}	$(c/c_{ m max})^2$	$(t/c)^{0}$
Stress from gravity	D^1	1	λ^2	B^1	$(c/c_{ m max})^{-1}$	$(t/c)^{0}$
Centrif. force/h	D^1	$V_{ m ave}^{-2}$	λ^0	B^{-1}	$(c/c_{ m max})^1$	$(t/c)^{0}$
Centrif. stress	D^0	$V_{ m ave}^{^{-2}}$	λ^2	B^0	$(c/c_{ m max})^0$	$(t/c)^0$
Flap frequency	D^{-1}	$V_{ m ave}^{^{^{^{^{^{^{^{^{^{^{^{^{^{^{^{^{^{^{$	λ^{-2}	B^{-1}	$(c/c_{ m max})^1$	$(t/c)^1$
Edge frequency	D^{-1}	$V_{ m ave}^{^{0}}$	λ^{-2}	B^{-1}	$(c/c_{ m max})^1$	$(t/c)^0$
Lock number $\cdot h$	D^1	$V_{ m ave}^{-1}$	λ^3	B^1	$(c/c_{ m max})^{-1}$	$(t/c)^{-1}$
		l thickness d	imensioned of	on extrem	e wind $V_{ m ref}$:	
$C_{ m drag}(90)$	1	1	$\lambda^{0.4}$	$B^{0.2}$	$(c/c_{ m max})^{-0.2}$	1
Aero force (parked)	D^2	$V_{ m ref}^{-2}$	$\lambda^{-1.6}$	$B^{-0.8}$	$(c/c_{ m max})^{0.8} \ (c/c_{ m max})^{0.8}$	1
M _{aero} (parked)	D^3	$V_{ m ref}^{\;2}$	$\lambda^{-1.6}$	$B^{-0.8}$	$(c/c_{ m max})^{0.8}$	1
Wall thickness h	D^1	$V_{ m ref}^{\;2}$	$\lambda^{2.4}$	$B^{1.2}$	$(c/c_{ m max})^{-1.2}$	$(t/c)^{-1}$
Bending stiffness	D^4	$V_{ m ref}^{2} \ V_{ m ref}^{2} \ V_{ m ref}^{2}$	$\lambda^{-3.6}$	$B^{-1.8}$	$\frac{(c/c_{\text{max}})^{-1.2}}{(c/c_{\text{max}})^{1.8}}$	$(t/c)^1$
Sectional mass	D^2	V_{rof}^{-2}	$\lambda^{0.4}$	$B^{0.2}$	$(c/c_{ m max})^{-0.2}$	$(t/c)^{-1}$ $(t/c)^{-1}$ $(t/c)^{-1}$
Total blade mass	D^3	$V_{ m ref}^{\;\;2}$	$\lambda^{0.4}$	$B^{0.2}$	$(c/c_{ m max})^{-0.2}$	$(t/c)^{-1}$
Rotor inertia	D^5	$V_{ m ref}^{\;\;2}$	$\lambda^{0.4}$	$B^{1.2}$	$(c/c_{ m max})^{-0.2}$	$(t/c)^{-1}$
Gravity moment	D^4	$V_{ m ref}^{2} \ V_{ m ref}^{2} \ V_{ m ref}^{2} \ V_{ m ref}^{2}$	$\lambda^{0.4}$	$B^{0.2}$	$(c/c_{\rm max})^{-0.2}$ $(c/c_{\rm max})^{-0.2}$ $(c/c_{\rm max})^{-0.2}$ $(c/c_{\rm max})^{-0.2}$	$(t/c)^{-1}$
Edgew. resistance	D^3	$V_{ m ref}^{-2}$	$\lambda^{-1.6}$	$B^{-0.8}$	$(c/c_{\rm max})^{0.6}$	$(t/c)^{-1}$
Stress from gravity	D^1	1	λ^2	B^1	$(c/c_{ m max})^{-1}$	$(t/c)^{0}$
Lock number	D^0	$rac{V_{ m ave}~V_{ m ref}^{-2}}{V_{ m ave}^{-3}}$	$\lambda^{0.6}$	$B^{-0.2}$	$(c/c_{ m max})^{0.2}$	$(t/c)^{0}$
Nominal Power	D^2	$V_{ m ave}^{-3}$?	?	?	?

For a number of properties this table gives the relation to some parameters. The first part of this table gives straightforward geometrical properties. The second part of this table also gives dependencies for a number of mechanical properties, for a constant wall thickness h. Assuming that the blade wall thickness is dimensioned on the extreme wind $V_{\rm ref}$ (which does not need to be the case) the third part of this table gives the final dependencies. For example, the blade flap frequency is proportional to: $\nu \approx V_{\rm ave} \cdot (c/c_{\rm max}) \cdot (t/c)/D/\lambda^2/B$. and expressed relative to the rotational speed (Per rev): $\nu \approx (c/c_{\rm max}) \cdot (t/c)/V_{\rm ave}/\lambda^3/B$. Note that for a given tip speed ratio the 'Per rev' flapping frequency does not scale with diameter D.

The dependency on the rotor speed Ω is implicitly described with the expression for the tip-speed-ratio $\lambda=\Omega\left(D/2\right)/V_{\rm ave}$.

Relations that have an explicit dependency on the rotor speed Ω instead of the tip-speed-ratio λ are given in the following table. Here it appears that the dependencies on diameter and wind velocity are different, see e.g. the first 5 lines in the tables.

	Diameter	Wind	Rotor	no. of	Rel. chord	Rel. airfoil
Property		speed	speed Ω	Blades	$c/c_{ m max}$	thickn. t/c
Tip sp. ratio λ	D^1	$V_{ m ave}^{-1}$	Ω^1	1	1	1
Rotor area	D^2	1	1	1	1	1
Blade chord c	D^{-1}	$V_{ m ave}^{\;2}$	Ω^{-2}	B^{-1}	$(c/c_{ m max})^1$	1
Blade area	D^0	$V_{ m ave}^{^{2}}$	Ω^{-2}	B^{-1}	$(c/c_{ m max})^1$	1
Aspect ratio	D^2	$V_{ m ave}^{-2}$	Ω^2	B^1	$(c/c_{ m max})^{-1}$	1
						_
		properties are				
Bending stiffness/h	D^{-3}	$V_{ m ave}^{\;\;6}$	Ω_{-6}	B^{-3}	$(c/c_{ m max})^3$	$(t/c)^{2}$
Sectional mass/h	D^{-1}	$V_{ m ave}^{-2}$	Ω^{-2}	B^{-1}	$(c/c_{ m max})^1$	$(t/c)^{0}$
Total blade mass/ h	D^0	$V_{ m ave}^{-2}$	Ω^{-2}	B^{-1}	$(c/c_{ m max})^1$	$(t/c)^{0}$
Rotor inertia/h	D^2	$V_{ m ave}^{2} \ V^{2}$	Ω^{-2}	B^0	$(c/c_{ m max})^1$	$(t/c)^{0}$
Gravity moment/h	D^1	$V_{ m ave}^{-2}$	Ω^{-2}	B^{-1}	$(c/c_{ m max})^1$	$(t/c)^{0}$
Edge. resistance/h	D^{-2}	$V_{ m ave}^{-4}$	Ω^{-4}	B^{-2}	$(c/c_{ m max})^2$	$(t/c)^{0}$
Stress from gravity	D^3	$V_{ m ave}^{-2}$	Ω^2	B^1	$(c/c_{ m max})^{-1}$	$(t/c)^{0}$
Centrif. force/h	D^1	$V_{ m ave}^{-2}$	Ω_0	B^{-1}	$(c/c_{ m max})^1$	$(t/c)^{0}$
Centrif. stress	D^2	$V_{ m ave}^{-2} \ V_{ m ave}^{-2}$	Ω^2	B^0	$(c/c_{ m max})^0$	$(t/c)^{0}$
Flap frequency	D^{-3}	$V_{ m ave}^{-2}$	Ω^{-2}	B^{-1}	$(c/c_{ m max})^1$	$(t/c)^{1}$
Edge frequency	D^{-3}	$V_{ m ave}^{-2}$	Ω^{-2}	B^{-1}	$(c/c_{ m max})^1$	$(t/c)^{0}$
Lock number · h	D^4	$V_{ m ave}^{-2}$	Ω_3	B^1	$(c/c_{ m max})^{-1}$	$(t/c)^{-1}$
	XX7:411	11 41 1 - 1				
- (00)	$D^{0.4}$	l thickness din	$\frac{1}{\Omega^{0.4}}$	$\frac{1}{B^{0.2}}$		1
$C_{ m drag}(90)$	$D^{0.4} D^{0.4}$	$V_{ m ave}^{-0.4}$	$\Omega^{-1.6}$	$B^{-0.8}$	$(c/c_{\rm max})^{-0.2}$	1
Aero force (parked)		$V_{ m ref}^{-2} V_{ m ave}^{-1.6}$			$(c/c_{\rm max})^{0.8}$	1
M _{aero} (parked)	$D^{1.4} \ D^{3.4}$	$V_{ m ref}^{-2} V_{ m ave}^{-1.6}$	$\Omega^{-1.6}$	$B^{-0.8}$	$(c/c_{\rm max})^{0.8}$	$\frac{1}{(1,1)^{-1}}$
Wall thickness h		$V_{\mathrm{ref}}^{2} V_{\mathrm{ave}}^{-2.4}$	$\Omega^{2.4}$	$B^{1.2}$	$(c/c_{\rm max})^{-1.2}$	$(t/c)^{-1}$
Bending stiffness	$D^{0.4}$	$V_{\rm ref}^{-2} V_{\rm ave}^{-3.6}$	$\Omega^{-3.6}$	$B^{-1.8}$	$(c/c_{\rm max})^{1.8}$	$(t/c)^1$
Sectional mass	$D^{2.4}$	$V_{ m ref}^{-2} V_{ m ave}^{-0.4}$	$\Omega^{0.4}$	$B^{0.2}$	$(c/c_{\text{max}})^{-0.2}$	$(t/c)^{-1}$
Total blade mass	$D^{3.4}$	$V_{ m ref}^{\ 2} V_{ m ave}^{\ -0.4}$	$\Omega^{0.4}$	$B^{0.2}$	$(c/c_{\rm max})^{-0.2}$	$(t/c)^{-1}$
Rotor inertia	$D^{5.4}$	$V_{ m ref}^{\ 2} V_{ m ave}^{\ -0.4}$	$\Omega^{0.4}$	$B^{1.2}$	$(c/c_{\rm max})^{-0.2}$	$(t/c)^{-1}$
Gravity moment	$D^{4.4}$	$V_{ m ref}^{\ 2} V_{ m ave}^{\ -0.4}$	$\Omega^{0.4}$	$B^{0.2}$	$(c/c_{\max})^{-0.2}$	$(t/c)^{-1}$
Edgew. resistance	$D^{1.4}$	$V_{ m ref}^{\ 2} V_{ m ave}^{\ 1.6}$	$\Omega^{-1.6}$	$B^{-0.8}$	$(c/c_{ m max})^{0.8}$	$(t/c)^{-1}$
Stress from gravity	D^3	$V_{ m ave}^{-2}$	Ω^2	B^1	$(c/c_{\max})^{-1}$	$(t/c)^{0}$
Lock number	D^0	$V_{ m ave} V_{ m ref}^{-2}$	$\Omega^{0.6}$	$B^{-0.2}$	$(c/c_{\rm max})^{0.2}$	$(t/c)^{0}$
Nominal Power	D^2	$V_{ m ave}^{-3}$?	?	?	?

In these tables the dependencies for the nominal power (and finally annual yield) are only included in terms of dimension and wind velocity, which follows also directly from the actuator disc theory.

The influence of tip-speed ratio on the nominal power is a non-linear function in which the airfoil drag and the tip-losses are involved. For the influence of the number of blades B on the power one definitely needs a more accurate model for tip-losses than the factor of Prandtl.